OXFORD

SOT | Society of Toxicology
academic.oup.com/toxsci

TOXICOLOGICAL SCIENCES, 174(1), 2020, 63–78

doi: 10.1093/toxsci/kfz238
Advance Access Publication Date: December 6, 2019
Research Article

Development of an *In Vitro* Human Thyroid Microtissue Model for Chemical Screening

Chad Deisenroth ,*,[1] Valerie Y. Soldatow,[†] Jermaine Ford,[‡] Wendy Stewart,* Cassandra Brinkman,* Edward L. LeCluyse,[†] Denise K. MacMillan,[‡] and Russell S. Thomas *

*National Center for Computational Toxicology, Office of Research and Development, U.S. Environmental Protection Agency, Research Triangle Park, North Carolina 27711; [†]LifeNet Health, Virginia Beach, Virginia 23453; and [‡]Research Cores Unit, Office of Research and Development, National Health and Environmental Effects Research Laboratory, Research Triangle Park, North Carolina 27711

[1]To whom correspondence should be addressed at National Center for Computational Toxicology, U.S. Environmental Protection Agency, Research Triangle Park, NC 27711. E-mail deisenroth.chad@epa.gov

Disclaimer: The views expressed in this article are those of the authors and do not necessarily reflect the views or policies of the U.S. Environmental Protection Agency. Mention of trade names or commercial products does not constitute endorsement or recommendation for use.

ABSTRACT

Thyroid hormones (TH) are essential for regulating a number of diverse physiological processes required for normal growth, development, and metabolism. The US EPA Endocrine Disruptor Screening Program (EDSP) has identified several molecular thyroid targets relevant to hormone synthesis dynamics that have been adapted to high-throughput screening (HTS) assays to rapidly evaluate the ToxCast/Tox21 chemical inventories for potential thyroid disrupting chemicals (TDCs). The uncertainty surrounding the specificity of active chemicals identified in these screens and the relevance to phenotypic effects on *in vivo* human TH synthesis are notable data gaps for hazard identification of TDCs. The objective of this study was to develop a medium-throughput organotypic screening assay comprised of reconstructed human thyroid microtissues to quantitatively evaluate the disruptive effects of chemicals on TH production and secretion. Primary human thyroid cells procured from qualified euthyroid donors were analyzed for retention of NK2 homeobox 1 (NKX2-1), Keratin 7 (KRT7), and Thyroglobulin (TG) protein expression by high-content image analysis to verify enrichment of follicular epithelial cells. A direct comparison of 2-dimensional (2D) and 3-dimensional (3D) 96-well culture formats was employed to characterize the morphology, differential gene expression, TG production, and TH synthesis over the course of 20 days. The results indicate that modeling human thyroid cells in the 3D format was sufficient to restore TH synthesis not observed in the 2D culture format. Inhibition of TH synthesis in an optimized 3D culture format was demonstrated with reference chemicals for key molecular targets within the thyroid gland. Implementation of the assay may prove useful for interpreting phenotypic effects of candidate TDCs identified by HTS efforts currently underway in the EDSP.

Key words: thyroid; organotypic culture model; thyroid disrupting chemicals; endocrine toxicology.

Statutes in the Food Quality Protection Act direct the U.S. Environmental Protection Agency (EPA) to test chemicals that may produce estrogenic effects in humans and has been expanded in scope in the Endocrine Disruptor Screening Program (EDSP) to evaluate other endocrine effects on androgen signaling, steroidogenesis, and thyroid function (EPA, 2014). Multiple organ systems in the body are dependent on sufficient thyroid hormone (TH) levels for regulating normal growth, development, and energy metabolism (Bassett and Williams, 2016; Brent, 2012; Forhead and Fowden, 2014; Li *et al.*, 2014; Lindsey *et al.*, 2018; Liu and Brent, 2018; McAninch and Bianco, 2014; Mullur *et al.*, 2014; Yang *et al.*, 2018). Primary hypothyroidism,

manifested as a decrease in thyroxine (T4) hormone and an increase in thyroid-stimulating hormone (TSH), is a particularly serious endocrine disorder during fetal and early-life stages that can result in irreversible adverse effects on brain and skeletal development (Auso *et al.*, 2004; Gilbert and Sui, 2008; Gothe *et al.*, 1999; Sharlin *et al.*, 2008; Zoeller and Crofton, 2000). The most widely recognized etiology of maternal or congenital hypothyroidism is iodine deficiency (De Benoist *et al.*, 2004), but gene mutations affecting thyroid development (Szinnai, 2014) or exposure to environmental contaminants (Boas *et al.*, 2006; Brucker-Davis, 1998; Miller *et al.*, 2009) also play a role. Disruption of serum TH levels across the hypothalamic-pituitary-thyroid (HPT) axis can occur through multiple postulated mechanisms including interference with hypothalamic-pituitary signaling, inhibition of TH synthesis and transport kinetics, metabolic clearance through the liver, and modulation of target tissue-dependent TH deiodination or receptor-mediated gene transactivation (DeVito *et al.*, 1999; Murk *et al.*, 2013; OECD, 2017).

Several Tier 1 and 2 test guideline assays in the EDSP evaluate thyroid weight, histopathology, and serum TH as *in vivo* endpoints for informing thyroid-specific adverse outcomes. The high cost, low-throughput capacity, and animal-dependent nature of these assays has spurred efforts by the EPA (2017) to develop a thyroid conceptual framework that outlines known thyroid-related pathways, identifies key molecular initiating events (MIEs) as likely targets for perturbation, and proposes a path forward to develop and apply a battery of *in vitro* assays for examining mechanisms across the HPT axis. Along these lines, high-throughput screening (HTS) assays for thyroperoxidase (TPO; Paul *et al.*, 2014; Paul Friedman *et al.*, 2016), sodium–iodide symporter (NIS; Hallinger *et al.*, 2017; Wang *et al.*, 2018, 2019), and deiodinase enzymes (DIO1, DIO2, and DIO3; Hornung *et al.*, 2018; Olker *et al.*, 2019) have been used to rapidly screen thousands of chemicals for potential disruption of TH synthesis. A limitation to these target-based approaches is the uncertainty in predicting tissue-level functional effects on TH production in a manner that is more physiologically relevant and analogous to endpoints evaluated in existing guideline studies. As a result, a tiered screening approach for hazard identification was developed in the EPA Computational Toxicology (CompTox) program where chemicals flagged in HTS assays with verified biological targets, such as those for thyroid-specific MIEs, are further evaluated in human organotypic cell culture models that may enable determination of relative potency relationships to apical endpoints commonly used for regulatory assessments (Thomas *et al.*, 2019). Given the complex regulation of TH homeostasis and uncertainty regarding the potential physiological effects of chemicals identified in thyroid HTS assays, there is a need to develop new approach methods that better recapitulate thyroid biology to identify hazards to thyroid function that may pose a risk to human health.

There is an inherent anatomically based, structure–function relationship in the thyroid gland not recapitulated in existing thyroid HTS assays that determines fidelity of hormone production. The gland is comprised of two independent lobes containing follicles that make up the functional units of the organ. Thyroid follicles are typically round or elongated structures of variable size that contain a single layer of follicular epithelial cells (thyrocytes) surrounding an internal lumen (Bianco *et al.*, 2014). To synthesize hormone, polarized thyrocytes generate a sodium gradient along the basolateral membrane that mediates uptake of iodide where it is translocated across the apical membrane into the thyroglobulin-rich follicular lumen to undergo oxidation and organification, leading to reuptake of iodothyronine hormone precursor that is enzymatically digested in lysosomes to produce mature T4 and 3,5,3′-triiodothyronine (T3). The functions ascribed to follicular units are dependent on this structural architecture to regulate TH synthesis and bioavailability (Colin *et al.*, 2013).

Cell-type selection plays a critical role in reproducing native functions of the thyroid. A number of thyroid-derived tumor cell lines are available, but due to the tumor-specific origin and extended passage in culture, these lines often result in an undifferentiated phenotype with loss of thyrocyte-specific gene expression, nonresponsiveness to TSH, and chromosomal abnormalities (van Staveren *et al.*, 2007). Immortalization of differentiated thyrocytes from rat (Ambesi-Impiombato and Villone, 1987; Brandi *et al.*, 1987; Fusco *et al.*, 1987), sheep (Aouani *et al.*, 1987), and human (Lemoine *et al.*, 1989) thyroid tissue have provided viable alternatives for the study of thyrocyte function, but with extended maintenance in long-term 2-dimensional (2D) cultures, these lines can result in clonal variants with phenotypic modifications as cells adapt to conventional culture conditions (Asmis *et al.*, 1996; Coppa *et al.*, 1995; Davies *et al.*, 1987; Huber *et al.*, 1990; Zimmermann-Belsing *et al.*, 1998). Short-term cultures of primary thyrocytes isolated from histologically normal thyroid glands often represent a better alternative to modeling thyroid function *in vitro* because primary thyrocytes have fully differentiated in their native environment, express the appropriate suite of genes necessary and sufficient for hormone synthesis, and have not yet acquired genetic or epigenetic modifications that often arise from long-term culturing (Eggo *et al.*, 1984; 1996; Ericson and Nilsson, 1996; Gerard *et al.*, 1989; Rapoport, 1976; Roger *et al.*, 1988, 1997; Westermark and Westermark, 1982). A number of experimental systems utilizing primary rat, porcine, and human thyrocytes have demonstrated that appropriate cell–matrix interactions in 3-dimensional (3D) systems can enhance cell polarity, increase responsiveness to TSH, promote increased expression of hormone-dependent genes, and in some cases, promote nascent synthesis of TH (Bernier-Valentin *et al.*, 2006; Chambard *et al.*, 1981; Garbi *et al.*, 1984; 1986; Kraiem *et al.*, 1991; Kusunoki *et al.*, 1995; 2001; Lissitzky *et al.*, 1971; Massart *et al.*, 1988; Mauchamp *et al.*, 1979; Thomas-Morvan *et al.*, 1988; Toda *et al.*, 1992).

Considerable progress in developing and applying HTS assays for thyroid-relevant MIEs has resulted in the identification of hundreds of potential thyroid disrupting chemicals (TDCs). An *in vitro* assay that simulates the structure–function relationship of the thyroid in a physiologically relevant manner and is amenable to evaluating chemical-dependent effects on TH biosynthesis may provide an orthogonal approach to evaluating the uncertainty associated with the candidate TDCs identified in HTS assays. The objective of this study was to develop a medium-throughput organotypic screening assay comprised of reconstructed human thyroid microtissues to quantitatively evaluate the disruptive effects of chemicals on TH production and secretion. Cells procured from qualified euthyroid human donors were analyzed for retention of NK2 homeobox 1 (NKX2-1), Keratin 7 (KRT7), and Thyroglobulin (TG) expression by high-content image analysis to verify enrichment of thyrocytes. A direct comparison of 2D and 3D 96-well culture formats was employed to evaluate morphology, differential gene expression, TG secretion, and TH synthesis over the course of 20 days (Figure 1A). Inhibition of TH synthesis in an optimized 3D culture format was demonstrated with reference chemicals for key MIEs within the thyroid gland. Implementation of the assay

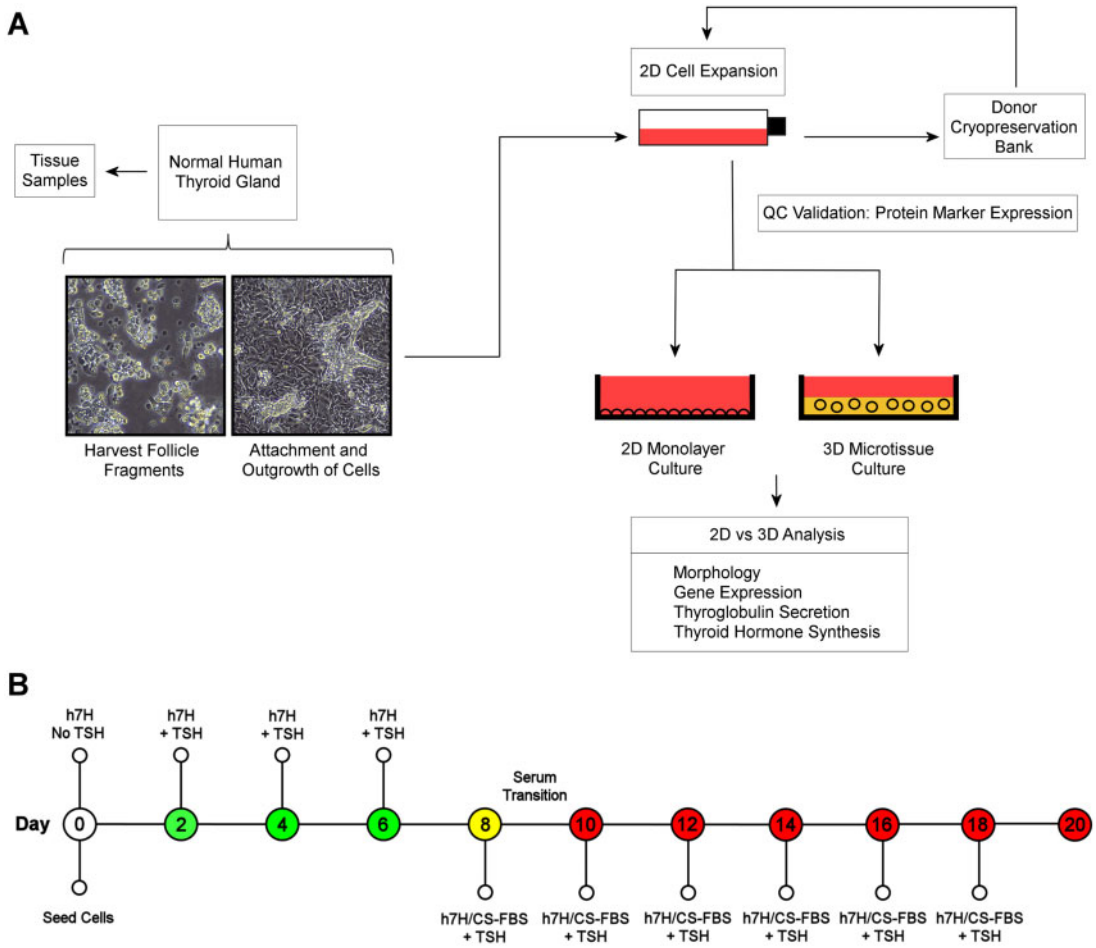

Figure 1. Overview of organotypic thyroid microtissue model development. Thyroid glands procured from qualifying euthyroid human donors were processed for cell isolation and matched tissue samples cryopreserved for RNA extraction. After limited expansion in 2D culture, the majority of cells were cryopreserved in a donor bank for subsequent experiments. Quality control (QC) validation was performed on a small subset of live isolates to ensure the cells met minimum technical specifications for sub-population enrichment. Model development entailed direct comparison of 2D and 3D culture formats for characterization of morphological and molecular endpoints, as well as functional evaluation of thyroglobulin secretion and thyroid hormone synthesis (A). Thyrocytes from live isolation or cryopreservation were seeded in 96-well 2D and 3D culture formats on day 0. Cells were cultured in h7H medium in standard FBS (days 0–8) or charcoal-stripped FBS (days 9–20) and medium exchanged every 2 days. Medium was supplemented with TSH from days 2–20 of the workflow (B).

may prove useful for interpreting tissue-level effects of candidate TDCs identified by HTS efforts currently underway in the EDSP.

MATERIALS AND METHODS

Human thyroid follicular epithelial cells. Primary human thyroid-derived cells and donor-matched tissue were obtained from LifeNet Health (Virginia Beach, Virginia). A panel of 8 human male donors used in this study were of Caucasian or African-American race, a mean age of 31 years (range: 17–66), a mean body mass index (BMI) of 28 (range: 19–37), and were of euthyroid status (Table 1). Serological testing was performed to confirm donors were negative for human immunodeficiency virus, and hepatitis B and C. Each donor lot of cells was used independently for the experiments described in this study.

The cold ischemic time from initial recovery flush to isolation of thyroid cells was $\leq$12 h. For cell isolation, tissues were removed from cold storage fluid and immersed in ice-cold Hank's Balanced Salt Solution (HBSS) in a large diameter Petri dish. Adipose and connective tissues were trimmed from the gland and washed again in HBSS. Remaining tissue was minced into 1–2 mm pieces and digested with a cocktail containing collagenase IV, collagenase IA, and trypsin (MilliporeSigma, St. Louis, MO) on an orbital shaker at 37°C and 5% CO_2 with periodic monitoring every 30–60 min for digestion progression. Undigested tissue fragments were allowed to settle and the top layer of digested material containing follicle fragments and cells was collected. Digestion was repeated in this manner until all

Table 1. Donor Specifications

Donor	LNH ID	Age	Gender	Race	BMI
1	1721880	32	M	Caucasian	22
2	1722161	21	M	Caucasian	32
3	1811621	66	M	African-American	35
4	1817005	27	M	Caucasian	19
5	1818646	31	M	Caucasian	31
6	1910289	18	M	Caucasian	22
7	1910552	36	M	Caucasian	37
8	1910594	17	M	African-American	27

LifeNet Health donor identification number (LNH ID) for all 8 euthyroid donors examined in this study. Specifications for age, gender, race, and BMI are noted.

fragments were digested. Each fraction was washed in HBSS, centrifuged at 200 × g for 5 min, and the cell pellet resuspended in humanized 7 homeostatic additives (h7H) medium. A viability enrichment step was performed using a density gradient fractionation technique. The viable cell band was isolated and cells counted using the trypan blue exclusion method. The purified cell preparation was seeded into T-75 cell culture flasks in h7H medium and incubated for 16 h at 37°C and 5% CO_2 in a humidified chamber to allow for cell attachment. Medium was exchanged, and cells incubated for an additional 48–72 h to facilitate initial outgrowth and adaptation to cell culture conditions. The passage 0 population was then collected for cryopreservation or used immediately for experiments. All experiments utilized cells from passage 0 to 2.

Cell culture medium formulation. Primary human thyroid-derived cells were maintained in h7H medium (Bravo *et al.*, 2013). Nutrient mixture F-12 Ham Coon's modified medium, bovine TSH, human recombinant insulin, somatostatin, hydrocortisone, growth hormone, apotransferrin, sodium iodide, sodium selenite, reduced L-glutathione, DL ± -α-tocopherol, DL-α-tocopherol acetate, sodium bicarbonate, and newborn calf serum (NCS) were obtained from MilliporeSigma (Burlington, Massachusetts). Fetal bovine serum (FBS) and penicillin-streptomycin-amphoterecin B were obtained from ThermoFisher Scientific (Waltham, Massachusetts). For experiments detecting TH, the NCS and FBS were replaced with charcoal-stripped FBS (h7H CS-FBS medium) obtained from ThermoFisher Scientific (Waltham, Massachusetts). Medium formulations were prepared in 1-L stock bottles, sterilized through 0.2 μM bottle top filters (Corning, Corning, New York), and used for up to 3 weeks.

Immunocytochemistry. Following post isolation recovery for each donor tissue, thyroid-derived cells were incubated for 48 h as 2D monolayers in 96-well black-walled, tissue culture (TC)-treated, optical bottom microplates (ThermoFisher Scientific, Waltham, Massachusetts). The cells were fixed in 4% paraformaldehyde for 30 min, washed one time in phosphate-buffered saline (PBS), and stored at 4°C prior to processing. Samples were permeabilized in 1% Triton-X 100 in PBS for 5 min at room temperature and washed one time with PBS. Blocking/quenching buffer (1% BSA and 22.52 mg/ml glycine in PBS/0.1% Tween 20) was added and samples incubated with gentle rocking for 30 min at room temperature. Samples were incubated with primary antibody at a dilution of 1:100 with gentle rocking for 18 h at 4°C, washed one time with PBS, and incubated with species appropriate Alexa Fluor 488 (AF488) fluorescent secondary antibody at a dilution of 1:500 for 1 h at room temperature in the dark. A list of antibodies is found in Supplementary Table 1. Cells were counterstained with Hoechst 33342 (10 μg/ml; ThermoFisher Scientific, Waltham, MA) for 10 min, washed one time with PBS, and sealed with optical film for image acquisition.

For morphological image analysis, day 10 cultures in 2D and 3D formats were processed in the same manner as for immunocytochemistry (ICC). After the blocking/quenching buffer step, F-actin and nuclei were simultaneously labeled with the fluorescent phallotoxin Alexa Fluor 488 Phalloidin (6.6 μM; ThermoFisher Scientific, Waltham, Massachusetts) and Hoechst 33342 (10 μg/ml), respectively, for 1 h at room temperature in blocking/quenching buffer. Cells were washed one time with PBS and sealed with optical film for image acquisition.

Microscopy. Routine culture monitoring was performed with an EVOS FL cell imaging system (ThermoFisher Scientific, Waltham, Massachusetts). For protein biomarker analysis, images were acquired on a Perkin Elmer Opera Phenix high-content imager (PerkinElmer, Waltham, Massachusetts) using a standard 20×, 0.4 NA air objective, and 4.4 mega pixel sCMOS camera. Independent channels for Hoechst 33342 (ex/405 nM; em/435-480 nM) and AF488 (ex/488 nM; em/500-550 nM) were collected across 9 fields per well. Image analysis was performed in the instrument-based Harmony software using Hoechst-stained nuclei as primary channel objects. The percent responders for each respective biomarker were quantified at the single-cell level, and well-level summary data extracted for 3 technical replicates from each respective donor. A total of 6 human donors (LNH 1722161, 1817005, 1818646, 1910289, 1910552, 1910594) were evaluated for validation of epithelial cell enrichment. For confocal imaging, microtissue images were collected in a 100 μM z-stack, at 10 μM intervals, using multi-color excitation and detection of Hoechst 33342 and AF488 with the Confocal Synchrony Optics dual view microlens-enhanced spinning disk setup on the Opera Phenix. Image processing and visualization were performed in Corel PaintShop Pro X6 v16.0.0.113 x64 (Corel, Ottawa, Canada).

Cell culture models. The 96-well black-walled, TC-treated, optical bottom microplates (ThermoFisher Scientific, Waltham, Massachusetts) were left uncoated (for 2D) or pre-coated (for 3D) with 50 μl of Matrigel with a protein concentration of approximately 10 mg/ml (Corning, Corning, New York). The plates were incubated at 37°C for 1 h to solidify Matrigel prior to use. Primary human thyroid-derived cells from passage 0–2 were dissociated using TrypLE Select (10×), no phenol red (ThermoFisher Scientific, Waltham, Massachusetts) for 10–20 min, centrifuged for 5 min at 200 × g in a swing bucket rotor, and gently resuspended in h7H medium. The cells were counted using the trypan blue exclusion method on a Countess automated cytometer (ThermoFisher Scientific, Waltham, Massachusetts). The cells were dispensed at 100 μl per well for a final seeding density of 3.0×10^4 cells/well and immediately placed in an incubator set at 37°C and 5% CO_2. Every 48 h the medium was reverse aspirated using an automated multichannel pipet and refed with h7H medium. Both the 2D and 3D models were incubated in this manner for the duration of culture to characterize morphology, differential gene expression, and thyroglobulin secretion (days 2–8), as well as iodotyrosine and TH production (days 10–20; Figure 1B).

Quantitative Real-Time PCR. For comparative gene expression analysis, total RNA was extracted from cells and donor-matched tissue using TRIzol reagent (ThermoFisher Scientific, Waltham, Massachusetts) and purified with the Qiagen RNeasy mini kit (Qiagen, Valencia, California). RNA was quantified on a NanoDrop spectrophotometer (NanoDrop Tech, Wilmington, Delaware) and a total of 100 ng used for qRT-PCR using the TaqMan RNA-to-CT 1-step kit (ThermoFisher Scientific, Waltham, Massachusetts). The following Human TaqMan probes (ThermoFisher Scientific, Waltham, Massachusetts) were used: Hs01053846_m1 (*TSHR*), Hs00794359_m1 (*TG*), Hs00892519_m1 (*TPO*), Hs00166567_m1 (*SLC5A5*), Hs00166504_m1 (*SLC26A4*), Hs00247586_m1 (*PAX8*), Hs00163037_m1 (*NKX2-1*), Hs00538731_s1 (*FOXE1*), Hs00213694_m1 (*DUOX1*), Hs00204187_m1 (*DUOX2*), Hs00328806_m1 (*DUOXA1*), Hs01595312_g1 (*DUOXA2*), and Hs00427620_m1 (*TBP*). Data were collected on a QuantStudio 7 Flex thermal cycler (ThermoFisher Scientific, Waltham, Massachusetts) and normalized to *TBP* to assess relative gene expression using the comparative Ct method. Normalized values were plotted as percent expression relative to donor-matched tissue.

Table 2. Reference Chemicals

Chemical name	CASRN	Molecular formula	Target	Classification
Dimethyl Sulfoxide	67-68-5	C_2H_6OS	—	Solvent control
Methimazole	60-56-0	$C_4H_6N_2S$	TPO	Antagonist
6-Propyl-2-thiouracil	51-52-5	$C_7H_{10}N_2OS$	TPO	Antagonist
Sodium Perchlorate	7601-89-0	$ClNaO_4$	NIS	Antagonist
VA-K-14 HCl	1171341-19-7	$C_{18}H_{16}ClN_3S$	TSHR	Antagonist
Benzophenone 3	131-57-7	$C_{14}H_{12}O_3$	—	Negative control

Chemicals with mechanisms of action for key molecular targets in the thyroid gland were selected as a reference set of thyroid disrupting compounds. Specifications for chemical name, CASRN, molecular formula, thyroid target protein, and classification are noted.

Enzyme-linked immunosorbent assays. Solid-phase enzyme-linked immunosorbent assays (ELISA; ThermoFisher Scientific, Waltham, Massachusetts) were used for the detection and quantification of human thyroglobulin protein (limit of detection: 220 pg/ml; Catalog #EHTG) or thyroxine hormone (limit of detection: 290 pg/ml; Catalog #EIAT4C) in the cell culture effluent. Analysis was conducted using conditioned h7H growth medium recovered from 96-well plates following a 48-h incubation period. ELISAs were performed according to the manufacturer's protocol. Data collection was conducted on a CLARIOstar microplate reader (BMG Labtech Inc, Cary, North Carolina). Concentrations of unknown samples and controls were interpolated from a standard curve fit with a 4-parameter nonlinear regression curve using MARS data analysis software v3.20 R2 (BMG Labtech Inc, Cary, North Carolina). Thyroglobulin samples were run at a dilution of 1:100 to fit within the linear range of the assay. Thyroxine samples were not diluted.

Liquid chromatography/tandem mass spectrometry. A previous method (Luna *et al.*, 2013) was used with modification to extract iodotyrosines (monoiodothyronine and diiodothyronine) and hormones (3,5-T2, 3,3′-T2, 3,5,3′-triiodothyronine, reverse T3, and thyroxine) from conditioned cell culture medium. Hormones were liberated from cell culture proteins by acid hydrolysis and purified using solid-phase extraction (SPE) on an Extrahera automated sample preparation unit (Biotage, Charlotte, North Carolina). For each sample, 40 µl of h7H medium was combined with 40 µl of 1 N HCl, 100 µl of organic-free reagent (OFR) water, 10 µl of 100 ng/ml internal standard mixture, and 120 µl of 50:50 mixture of OFR water: acetonitrile in a 96-well polypropylene deep well plate. Samples were vortexed and incubated at 37°C for 2 h in an air incubator. After cooling to room temperature, 300 µl of 0.1% acetic acid (aq) was added. Extraction was conducted with a mixed-mode Evolute Express CX cation exchange extraction plate (Biotage, Charlotte, North Carolina). Polar interferences were washed from the extraction plate by applying 400 µl of 0.1% acetic acid, followed by a final wash with 400 µl of methanol. Hormones were eluted from the extraction plate with 3 volumes (300 µl each) of 2.5% ammonium hydroxide in methanol (vol/vol). Sample extracts were evaporated to dryness using an SPE Dry 96 plate dryer (Biotage, Charlotte, North Carolina) and reconstituted in 100 µl of 0.1% formic acid in 95:5 OFR water:acetonitrile for analysis.

Instrumental analysis was performed on an ExionLC AC UHPLC-Qtrap 6500+ Linear Ion Trap liquid chromatography/tandem mass spectrometer (LC/MS/MS) system (Sciex, Framingham, Massachusetts). Chromatographic separation of the hormones was performed using a Raptor Biphenyl column (2.6 µm, 100 mm × 2.1 mm; Restek, Bellefonte, Pennsylvania). The oven temperature was set to 45°C, autosampler temperature held at 15°C, and sample volume of 15 µl injected. A linear gradient using 0.1% formic acid in water as mobile phase A and 0.1% formic acid in methanol as mobile phase B was used at a flow rate of 0.4 ml/min. The starting composition was 95% mobile phase A and 5% mobile phase B. After 1 min, the gradient was ramped to 95% mobile phase B over 5 min and held for 3 min. The column was re-equilibrated to starting conditions for 2 min for a total run time of 10 min. TH were detected by multiple reaction monitoring in positive-ion electrospray ionization mode operated with an IonDrive TurboV source. The source parameters were 35 psi for the curtain gas, 5.5 kV for the ion spray voltage, 500°C for the source temperature, 35 psi for both gas 1 and gas 2. Maximum sensitivity was achieved by optimizing each analyte separately and obtaining individual declustering potentials, entrance potentials, collision energies, and exit cell potentials (Supplementary Table 7).

Reference chemical evaluation. Methimazole (CASRN 60-56-0), 6-propyl-2-thiouracil (CASRN 51-52-5), sodium perchlorate (CASRN 7601-89-0), benzophenone 3 (CASRN 131-57-7), and dimethyl sulfoxide (CASRN 67-68-5) were obtained from MilliporeSigma (Burlington, Massachusetts). VA-K-14 HCl (CASRN 1171341-19-7) was obtained from Glixx Laboratories (Hopkinton, Massachusetts; Table 2). The 3D microtissue model was setup, as described, with continuous exposure to 1 mU/ml TSH for a duration of 8 days in h7H medium with standard FBS, transitioned for 2 days in h7H CS-FBS medium, then dosed with compound on days 10 and 12, with final conditioned medium sample collection on day 14. All compounds were administered across a log-fold titrated dose-range of 10 pM to 100 µM, in plate-based technical duplicate, for a total of 4 experimental replicates ($n = 4$) from a single donor. Thyroxine levels were measured by ELISA, as described. After sample collection, cytotoxicity was concurrently evaluated by measuring cellular ATP levels at day 14 using CellTiter-Glo 2.0 (Promega, Madison, Wisconsin) according to manufacturer's protocol with data collection conducted on a CLARIOstar microplate reader (BMG Labtech Inc, Cary, North Carolina).

For data analysis, plate-level technical replicates were normalized to the mean of plate-based DMSO solvent controls and mean normalized values plotted independently for each experiment. An ordinary one-way ANOVA with Dunnett's multiple comparison test was conducted to determine statistical significance at $p \leq .05$ for both the TH and cytotoxicity endpoints. A 3-parameter Hill model was fit to chemicals with statistically significant decreases in T4 levels, up to the highest viable concentration tested, and used to derive the half-maximal inhibition concentration (IC_{50}).

Data analysis. All data were plotted, visualized, and analyzed using GraphPad Prism v7.0 (GraphPad Software, La Jolla, California). Specific data normalization and statistical analyses

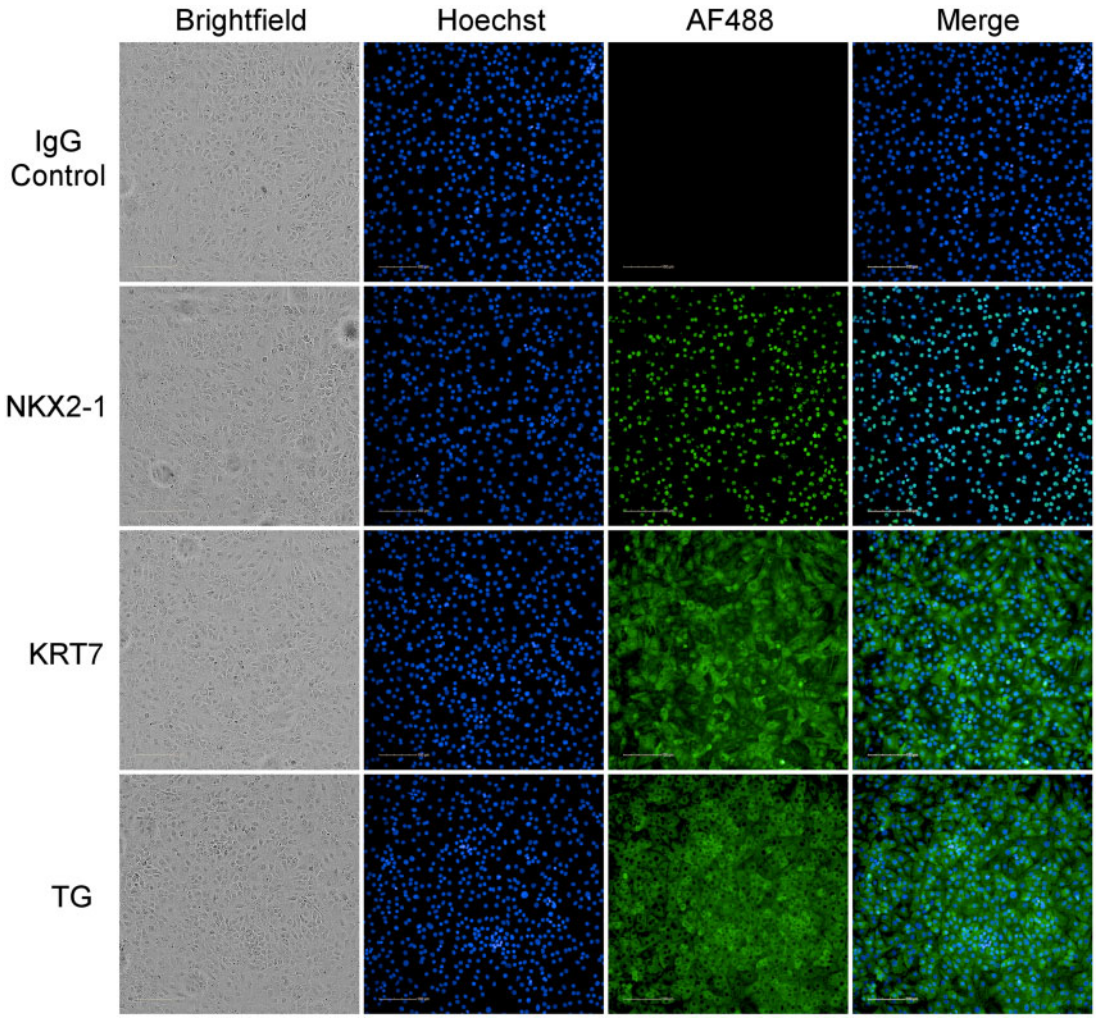

Figure 2. post isolation immunocytochemistry of thyroid-derived cells in 2D culture. Representative thyrocytes derived from passage 0 live cultures were seeded in 96-well microplates for 48 h. Immunostaining was performed for IgG isotype controls (α-Mouse IgG kappa is shown), NK2 Homeobox 1 (NKX2-1), Keratin 7 (KRT7), and Thyroglobulin (TG). Whole cell (Brightfield), cell nuclei (Hoechst 33342), target protein (AF488), and merged image (Hoechst 33342/AF488) are shown. Scale bar is 100 μM.

for each experiment are described within the methods and figure legends.

RESULTS

Thyroid Cell Isolation and Characterization

Thyroid tissue procured from qualified euthyroid donors were seeded for plating and expansion with an initial adaptation period of 48–96 h. Live isolates (passage 0) of each donor were harvested and directly plated for analysis in 2D monolayer culture to examine retention of NKX2-1, KRT7, and TG protein expression using ICC and high-content image analysis. These 3 biomarkers, in combination, confer relative specificity to thyroid follicular epithelial cells (Fagerberg, 2014; Gerard *et al.*, 1989; Nilsson and Fagman, 2017). As expected, NKX2-1 staining was predominantly nuclear-localized, whereas TG was restricted to the cytosol, and KRT7 exhibited mixed subcellular distribution. No consistent signal for IgG control antibodies was observed, indicative of low background signal (Figure 2). Image-analysis algorithms were developed and applied independently for each target-specific protein to quantitatively determine donor-dependent frequency and staining specificity ($n = 6$; Table 3). Analyses revealed a cell-level protein expression frequency of 95.18 ± 1.74% for NKX2-1 and 1.91 ± 0.50% for IgG isotype control. KRT7 was 90.52 ± 2.47% with low IgG kappa background of 0.3 ± 0.14%. TG was more variable at 53.37 ± 16.10%, but IgG kappa was low at 1.93 ± 1.31%. Collectively, characterization of these key expression markers in early passage cells was deemed sufficient for enriching for thyroid follicular epithelial cell populations that would be suitable for culture modeling across multiple donors.

Morphological Characterization

The extracellular matrix (ECM) provides mechanical, structural, and compositional cues to modulate cellular behavior (Humphrey *et al.*, 2014). In the case of thyrocytes, appropriate cell–matrix interactions in 3D systems have been observed to enhance thyrocyte organization and function (Bernier-Valentin *et al.*, 2006; Chambard *et al.*, 1981; Garbi *et al.*, 1984; 1986; Kraiem *et al.*, 1991; Kusunoki *et al.*, 1995; 2001; Lissitzky *et al.*, 1971; Massart *et al.*, 1988; Mauchamp *et al.*, 1979; Thomas-Morvan *et al.*, 1988; Toda *et al.*, 1992). To circumvent potential reduction of the thyrocyte phenotype in 2D culture, attempts were made to model the cells in a 3D environment to determine if primary

Table 3. Biomarker Image Cytometry

	IgG			IgG, kappa			NKX2-1			KRT7			TG		
Biomarker	% POS	SEM	N	% POS	SEM	N	% POS	SEM	N	% POS	SEM	N	% POS	SEM	N
NKX2-1	1.91	0.50	6	—	—	—	95.18	1.74	6	—	—	—	—	—	—
KRT7	—	—	—	0.30	0.14	6	—	—	—	90.52	2.47	6	—	—	—
TG	—	—	—	1.93	1.31	6	—	—	—	—	—	—	53.37	16.10	6
Donors LNH 1722161, 1817005, 1818646, 1910289, 1910552, 1910594															

The cell-level frequency of IgG isotype controls (α-Mouse IgG kappa and α-Rat IgG), NK2 Homeobox 1 (NKX2-1), Keratin 7 (KRT7), and Thyroglobulin (TG) staining were quantitatively evaluated by high-content imaging across 6 independent human donors for verification of thyroid follicular epithelial cell enrichment. Data are the summary statistics presented as mean % positive (% Pos) ± SEM ($n = 6$).

thyrocytes could self-organize into native follicle-like structures. Thus, thyrocytes were seeded onto a Matrigel hydrogel and allowed to incubate overnight. After a single day in culture, there was significant self-assembly into small microtissues of varying shapes and sizes of approximately 20–100 μM in diameter. After 10 days in culture, the 3D microtissues adopted a circular, hemispherical morphology with well-defined ridges and actin-dense center rings. In contrast, the 2D monolayers retained more homogenous nuclear spatial patterning and disorganized actin filaments reminiscent of a typical confluent monolayer (Figure 3A). Confocal analysis of a 3D microtissue at 10 days revealed a concentration of cells at the matrix interface that morphed into a follicle-like structure with internal pockets devoid of cells resembling luminal cavities (Figure 3B). When exposed to variable concentrations of TSH (0, 1, 5 mU/ml), 2D monolayers continued proliferating, forming confluent monolayers over the surface of the well. In contrast, 3D cultures exhibited visibly larger cell aggregates when exposed to TSH, but overall had visibly reduced outgrowth in the well over time as compared with monolayer cultures (Supplementary Figure 1A). The observation was supported by reduced ATP recovery in 3D cultures than 2D counterparts at day 20 (Supplementary Figure 1B). The results suggest primary thyrocytes in 2D culture maintain a proliferative state until reaching contact inhibition, whereas 3D microtissue aggregates undergo more limited proliferation, but remodel into more native follicle-like architecture.

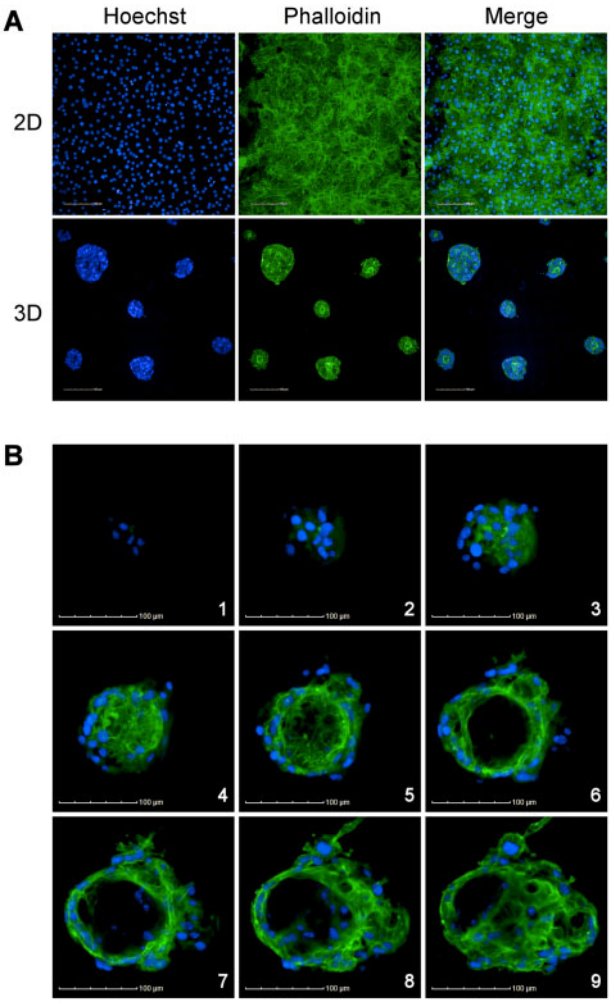

Figure 3. Morphological assessment of 2D monolayers and 3D microtissues. Day 10 cultures stained with Hoechst 33342 (blue) and Phalloidin conjugated to Alexa Fluor 488 (green) were used to evaluate the nuclei and actin cytoskeleton, respectively (A). Follicle-like morphology of a 3D microtissue at day 10 of culture visualized with confocal microscopy. Panels 1–9 are a bottom-to-top visualization of a single microtissue (B). Scale bar is 100 μM.

Gene Expression

The transcription factors *PAX8*, *NKX2-1*, and *FOXE1* play pivotal roles in regulating thyrocyte differentiation and function (Nilsson and Fagman, 2017). To evaluate the differentiation state of the cells in each model format, expression of each transcription factor was analyzed from a single donor (LNH1817005) relative to donor-matched thyroid tissue across 3 TSH exposure groups (0, 1, and 5 mU/ml; Figure 4; Supplementary Table 2). *PAX8* and *NKX2-1* expression were significantly more elevated in the 3D model at all 3 TSH exposure groups representing 20–30% of tissue-level controls. *FOXE1* expression was greater in the absence of TSH in the 3D format but suppressed in the presence of TSH relative to the 2D model. No TSH-dependent changes for any of the genes were noted in the 3D model, consistent with the TSH-independent nature of follicular morphogenesis (Postiglione *et al.*, 2002). These results indicate that the transcriptional regulation of thyrocyte differentiation is significantly impacted by the culture format, where 3D microtissue aggregates cultured on the hydrogel promote a more differentiated phenotype.

TSH activation of the TSH receptor (TSHR) on the basolateral membrane of thyrocytes initiates an intracellular signaling cascade that coordinates cellular functions involved in iodide uptake, TG expression, and TH production (Kopp and Solis-S, 2009). The impacts of TSH exposure were evaluated for essential hormone synthesis genes (*TSHR*, *TG*, *TPO*, *SLC5A5*, *SLC26A4*, *DUOX1*, *DUOX2*, *DUOXA1*, *DUOXA2*) where *TSHR* transcript levels

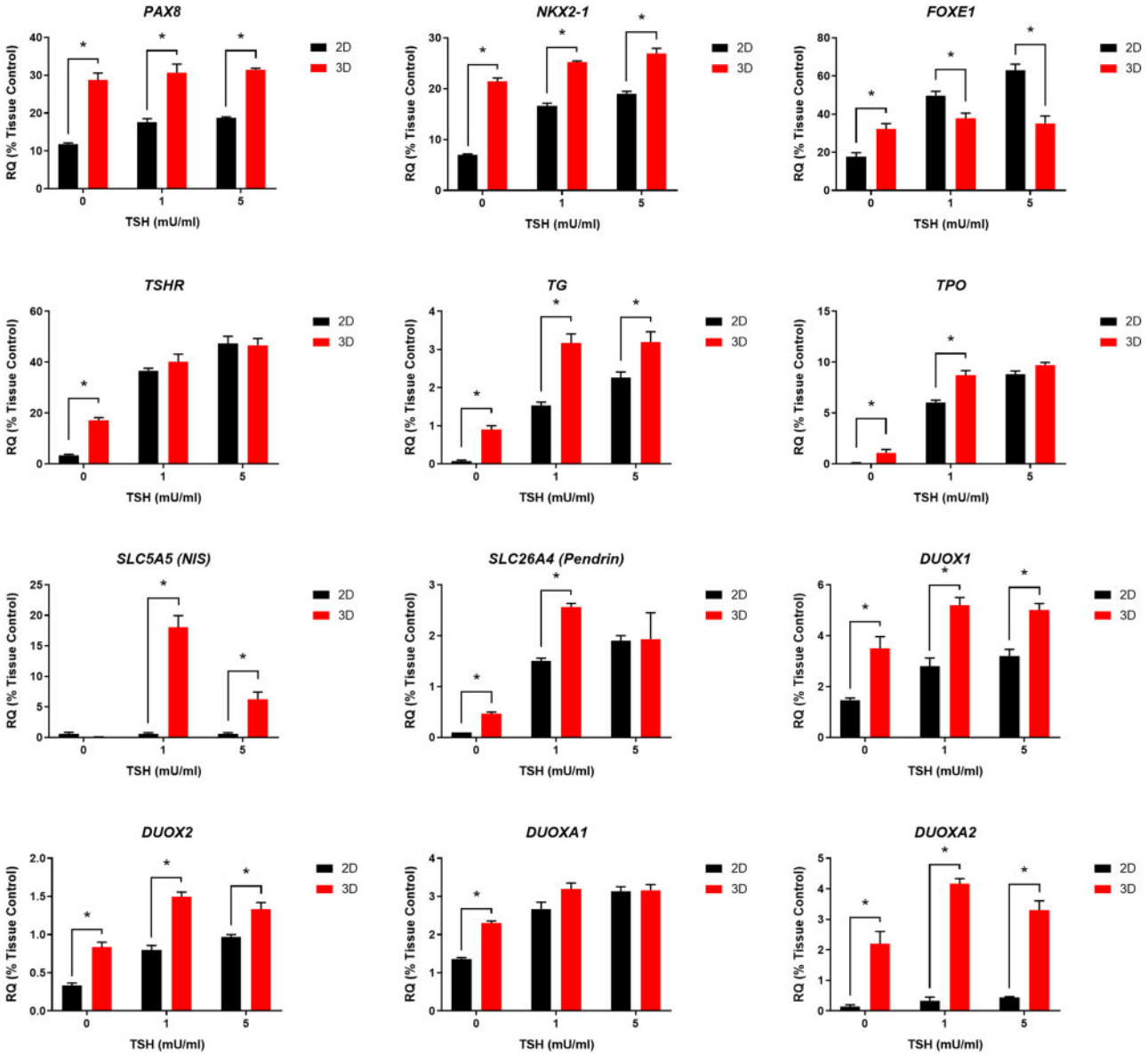

Figure 4. Gene expression profiling of 2D monolayers and 3D microtissues. Quantitative RT-PCR was used to profile markers for differentiation (*PAX8*, *NKX2-1*, *FOXE1*) and thyroid hormone biosynthesis (*TSHR*, *TPO*, *TG*, *SLC5A5*, *SLC26A4*, *DUOX1*, *DUOX2*, *DUOXA1*, *DUOXA2*) at day 8 of culture. Medium was supplemented with different concentrations (0, 1, 5 mU/ml) of TSH from days 2–8 of culture. 2D (black) and 3D (red) sample data were normalized to internal reference control (*TBP*) and expressed as the relative quantity (RQ) percentage to donor-matched tissue. Data are mean ± SEM of 3 experimental replicates ($n = 3$) from a single donor. Unpaired *t*-tests for each 2D and 3D pair-wise combination of raw dCT values in each TSH exposure group were used to determine statistical significance at $p \leq .05$.

were significantly higher in the 3D cultures, relative to the 2D, in the absence of TSH, but increased in both 2D and 3D formats when the medium was supplemented with TSH. *TG* and *TPO*, 2 TSH-dependent target genes, demonstrated concentration-dependent responses in both formats and were considerably higher in the 3D model. Interestingly, the basal membrane iodide transporter *SLC5A5* (*NIS*) was primarily detected in the 3D culture model only when TSH was present. To a lesser extent, *SLC26A4* (*Pendrin*), the apical membrane iodide transporter, was also more highly expressed in the 3D than 2D model at 0 and 1 mU/ml TSH conditions. The dual oxidases *DUOX1* and *DUOX2*, proteins normally present along the apical boundary of the follicle lumen, had higher expression in the 3D model in all 3 TSH exposure groups. In addition, the dual oxidase maturation factors exhibited differential expression, with *DOUXA2* exhibiting markedly higher levels in the 3D culture format. Collectively, the results demonstrate the microtissues present in the 3D model were more responsive to TSH exposures and expressed genes critical for TH production (eg *SLC5A5* and *DUOXA2*) not observed in the 2D cultures.

Thyroglobulin Protein Production

Intrinsic to the biosynthesis of TH is TG; a large 660 kDa dimeric protein induced by TSHR activation that serves as the scaffold for iodothyronine hormones (Citterio *et al.*, 2019). To determine functional differences in sensitivity of TSHR activation between the model types, TG protein production was monitored in the cell culture effluent of early passage thyrocytes from a single donor (LNH1817005). Thyrocytes were seeded in the absence of

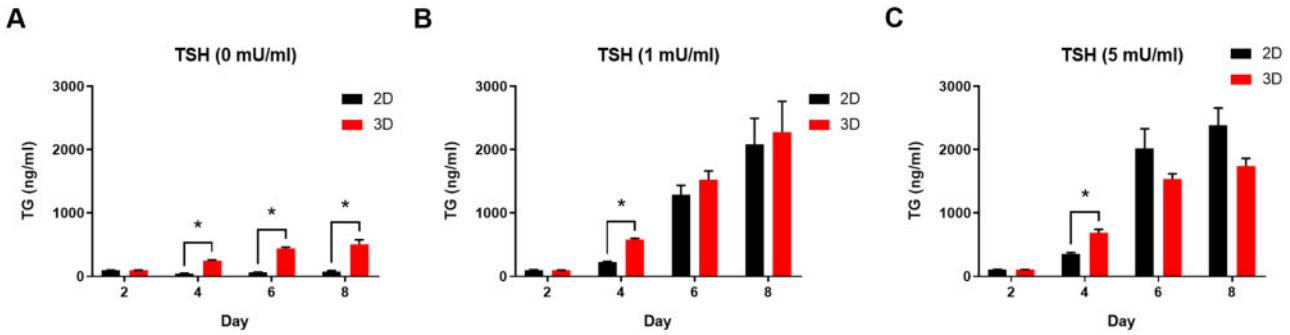

Figure 5. TSH-induced thyroglobulin secretion in 2D monolayers and 3D microtissues. Thyroglobulin protein secretion was measured from 2D (black) and 3D (red) cultures exposed to 0 mU/ml (A), 1 mU/ml (B), and 5 mU/ml (C) TSH concentrations from days 2–8 of culture. Thyroglobulin concentrations (ng/ml) are mean ± SEM of 4 experimental replicates ($n = 4$) from a single donor. Unpaired *t*-tests for each 2D and 3D pair-wise combination in each TSH exposure group were used to determine statistical significance at $p \leq .05$.

TSH for 2 days, then conditioned medium was sampled at days 2, 4, 6, and 8 across variable TSH concentrations (0, 1, or 5 mU/ml; Supplementary Table 3). At the day 2 baseline time point in 2D cultures, mean TG levels were comparable between 2D and 3D cultures. Even in the absence of TSH, 3D cultures continued to produce more TG over days 4–8, whereas 2D cultures remained at relative baseline (Figure 5A). When TSH was supplemented in the medium there was marked induction that increased in a time-dependent manner for both 2D and 3D models at 1 and 5 mU/ml (Figure 5B and 5C). Notably, the levels were significantly different across all 3 TSH-treatment groups at day 4, suggesting higher potential for TSH responsiveness in the 3D model. The results demonstrate that early passage thyrocytes retain sensitivity to TSH stimulation during the initial 8 days of culture in both formats, but have higher sensitivity in 3D microtissue culture, particularly at earlier time points.

TH Synthesis

Given the observations of native follicle-like morphology of the 3D microtissues, and TSH-dependent effects on gene expression and TG production, serial sampling of conditioned cell culture effluent was evaluated for accumulation of nascent TH from 3 independent donors (LNH1722161, LNH1818646, and LNH1910594) across days 10–20 of culture (Figure 6; Supplementary Table 4). TH synthesis begins with organification of intracellular iodide where thyroperoxidase-catalyzed oxidation and iodination of 1 or 2 positions in tyrosyl residues present in TG protein form monoiodothyronine (MIT) or diiodothyronine (DIT), respectively (Koibuchi, 2018). MIT was not detectable above background medium levels in 2D culture but was sufficiently detected in 3D culture in the presence of 1 and 5 mU/ml TSH (Figure 6A). Likewise, DIT was also detected in 3D culture in the presence of TSH, but not in 2D culture (Figure 6B).

Coupling of MIT and DIT iodotyrosine residues form the hormone precursors that undergo proteolytic cleavage to the major TH T3 and T4 (Koibuchi, 2018). Consistent with appearance of MIT and DIT in 3D cultures, T3 levels were detectable from days 10–20 only when cultures were exposed to TSH, exhibiting mean ranges of 2700–3792 pg/ml (1 mU/ml TSH) and 1762–3461 pg/ml (5 mU/ml TSH; Figure 6C). T4, the major product of thyroid-directed hormonogenesis, was also present in 3D cultures with a mean range of 8741–9311 pg/ml (1 mU/ml TSH) and 6250–7934 pg/ml (5 mU/ml TSH; Figure 6D). Despite robust expression of TG transcript (Figure 4) and protein (Figure 5), neither T3 nor T4 were observed in 2D cultures, indicating deficiency for key hormone production components in this culture format.

Type I and II deiodinase enzymes present in thyroid and peripheral tissues catalyze the conversion of T4 to active T3, whereas the type III deiodinases, and type I to a lesser extent, inactivate TH to reverse T3 (rT3) and to the diiodothyronines 3,5-T2 and 3,3′-T2 (Kohrle, 1999). None of the inactive TH products (rT3, 3,5-T2, 3,3′-T2) were appreciably detected in either culture format (Supplementary Figure 2). Type III deiodinase enzymes are not normally expressed in the thyroid (Kohrle, 1999), so the absence of these products suggests TH inactivation by deiodinases may not be a prominent mechanism of TH regulation in this culture model. However, type I deiodinase expression is TSH-dependent (Kohrle, 1999) and may contribute to the variability observed in T3 outputs across donors.

The presence of iodotyrosines and hormones from 3 independent donors indicates the 3D microtissue culture model is competent for hormonogenesis when stimulated by TSH. Considerable variation was observed for some values between donors (eg MIT and T3), but overall, the mean values for the dominant TH product T4 were primarily stable across the 10-day sampling period. Taking into account the high viability of cultures at day 20 (Supplementary Figure 1), these results demonstrate the suitability of the 3D microtissue culture model for long-term *in vitro* monitoring of TH biosynthesis.

Reference Chemical Evaluation of TH Disruption in a 3D Culture Model

The structural and functional characterization data supported implementation of the 3D culture model as a tool for evaluating the disruptive potential of chemicals on TH biosynthesis. Assay suitability was investigated by selecting reference chemicals with targeted mechanisms of action across key molecular components of the TH biosynthesis pathway. Established antagonists of TPO (methimazole and 6-propyl-2-thiouracil), NIS (sodium perchlorate), and TSHR (VA-K-14 HCL) were selected. Benzophenone 3, an inactive derivative of the potent TPO inhibitor benzophenone 2 (Paul *et al.*, 2014; Schmutzler *et al.*, 2007), was used as a negative control. All compounds were dissolved in DMSO and tested across an 8-point dilution series spanning 10 pM to 100 μM. For the 3D culture format, microtissues derived from a single donor (LNH1910594) were matured for 10 days, then exposed in 2-day dosing intervals for a total duration of 4 days. At day 14, culture effluent was collected for quantitative T4 determination (Supplementary Table 5) and post exposure

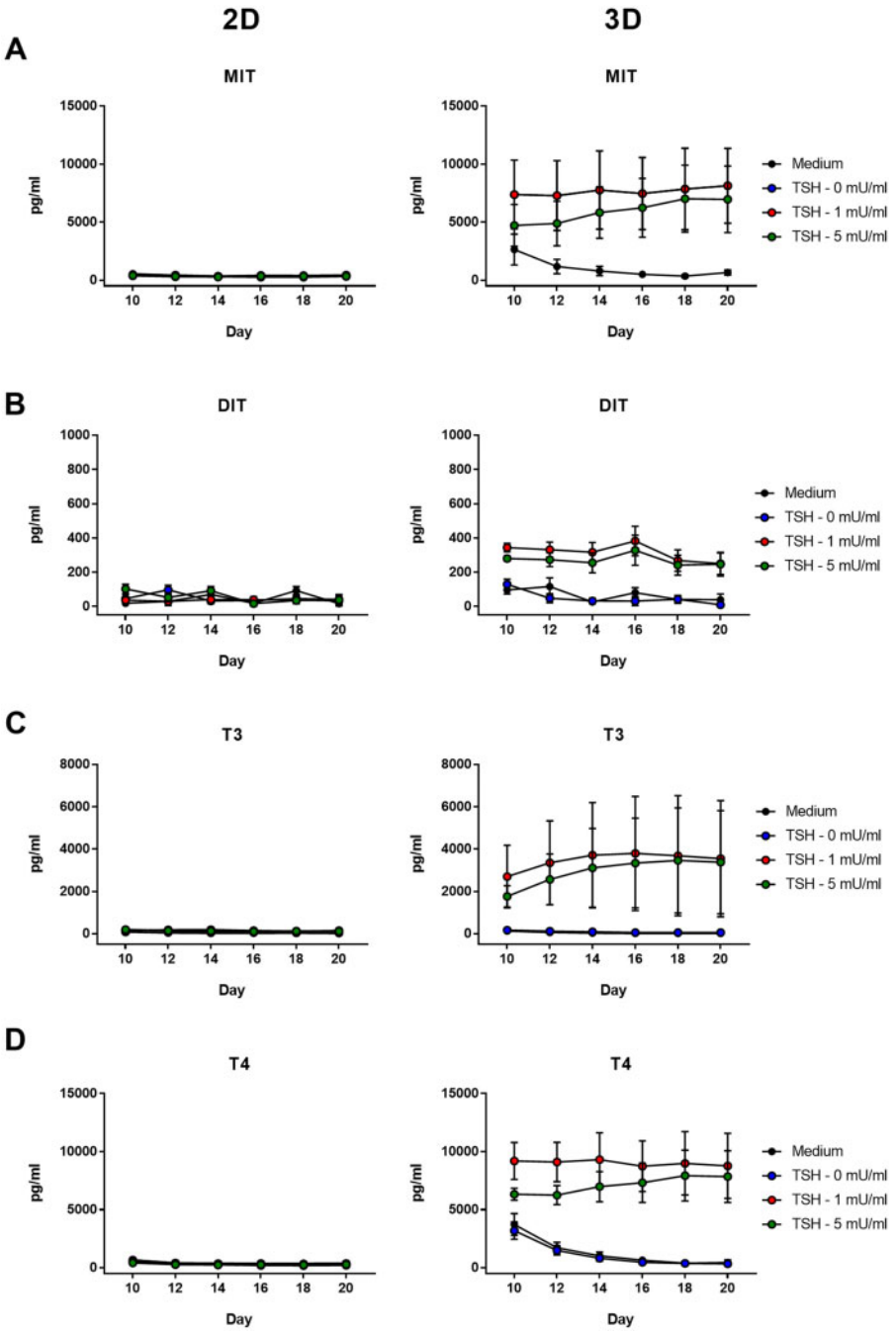

Figure 6. Thyroid hormone secretion in 2D and 3D culture models. Thyrocytes seeded from passage 0 live-isolate cultures were periodically monitored for (A) Monoiodothyronine (MIT), (B) Diiodothyronine (DIT), (C) 3,5,3′-Triiodothyronine (T3), and (D) Thyroxine (T4) accumulation from days 10–20 of culture. Analytes were measured by LC/MS/MS from conditioned h7H culture medium collected in 2-day intervals from samples exposed to 0, 1, or 5 mU/ml TSH. Plate-based culture medium from control wells with no cells (Medium) was used for background measurements in both culture formats. Data are mean ± SEM of a single experimental replicate from 3 independent donors ($n = 3$).

viability assessment on exposed microtissues (Supplementary Figure 3 and Table 6).

T4 hormone levels, normalized to plate-based DMSO solvent controls, were normally distributed with a coefficient of variation of 17.9%, indicating acceptable sampling variability ≤20% (Figure 7A). Methimazole (IC_{50}: 0.129 μM) significantly reduced T4 output to 53.0% at the maximum effect level relative to DMSO controls (Figure 7B). 6-Propyl-2-thiouracil (IC_{50}: 0.172 μM) had similar effects with maximum inhibition at 49.3% of solvent controls (Figure 7C). The NIS inhibitor, sodium perchlorate (IC_{50}: 3.233 μM), was less potent with T4 levels dropping to 60.5% of control (Figure 7D). VA-K-14 (IC_{50}: 5.614 μM) was cytotoxic at the highest concentration (Supplementary Figure 3) but significantly reduced T4 levels to 72.3% of control at the 1 μM concentration (Figure 7E). As expected, the negative control compound benzophenone 3 did not significantly reduce T4 output (Figure 7F) during the exposure period. Summary values for chemical potency (IC_{50}), maximum efficacy (E_{max}), and lowest

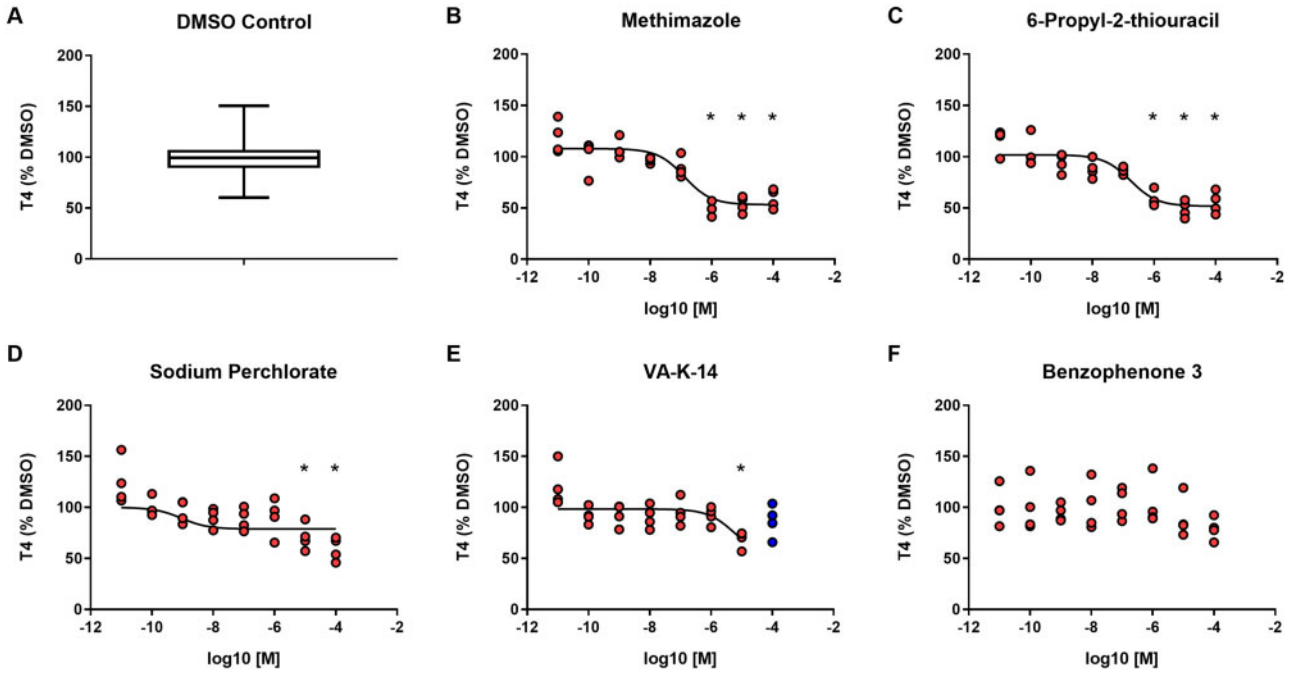

Figure 7. Evaluation of reference chemical inhibition of thyroid hormone synthesis in a 3D microtissue culture model. Human thyroid microtissues were matured in a 96-well 3D culture model for 10 days with exposure to 1 mU/ml TSH starting at day 2. Reference chemicals targeting TPO (Methimazole, 6-Propyl-2-thiouracil), NIS (Sodium Perchlorate), TSHR (VA-K-14), or negative control (Benzophenone 3) were administered in concentration response (10 pM to 100 μM) at days 10 and 12, for a total exposure duration of 4 days. Conditioned medium was collected on day 14 to measure thyroxine (T4) concentrations, with cytotoxicity concurrently evaluated by measuring cellular ATP levels. Values were normalized to plate-based solvent controls (DMSO) and plotted across experimental replicates ($n = 4$) from a single donor. An ordinary one-way ANOVA with Dunnett's multiple comparison test was conducted to determine statistical significance at $p \leq .05$. Test compound concentrations deemed significant are denoted by an asterisk. A 3-parameter Hill model was fit to chemicals with significant T4 depletion, up to the highest viable concentration tested, and used to derive the half-maximal inhibition concentration (IC_{50}). Plate-based mean T4 levels (red) and cytotoxic concentrations (blue) are shown.

Table 4. Reference Chemical Evaluation for Thyroid Disruption

Chemical	IC_{50} (μM)[a]	E_{max} (% T4)[b]	LEC (μM)[c]
Methimazole	0.129	53.0	1
6-Propyl-2-thiouracil	0.172	49.3	1
Sodium Perchlorate	3.23	60.5	10
VA-K-14 HCl	5.61	72.3	10
Benzophenone 3	—	—	—

Thyroid disrupting chemicals screened for inhibition of thyroxine (T4) synthesis.
[a]Half-maximal inhibition concentration (IC_{50}) derived from the curve fit.
[b]Maximum effect (E_{max}) observed for mean T4 accumulation relative to DMSO solvent controls (% T4).
[c]Lowest effect concentration (LEC) deemed significant at $p \leq .05$.

significant effect concentration (LEC) are noted in Table 4. Given the 3D model recapitulates a broad array of MIEs integral to TH biosynthesis, validation by these reference antagonists demonstrates utility in anchoring target-specific effects to an apical hormone phenotype with physiological human relevance.

DISCUSSION

Considerable progress has been made in the development and application of HTS assays for thyroid-related MIEs, resulting in the identification of hundreds of potential TDCs (Hallinger *et al.*, 2017; Hornung *et al.*, 2018; Olker *et al.*, 2019; Paul *et al.*, 2014; Paul Friedman *et al.*, 2016; Titus *et al.*, 2008; Wang *et al.*, 2018, 2019). An *in vitro* screening model that better recapitulates the intrinsic biology of the thyroid gland may prove useful for orthogonal confirmation of tissue-level effects on the TH biosynthesis pathway, thus reducing the uncertainty associated with HTS assays. In this study, primary human thyrocytes isolated from euthyroid donors were used to conduct parallel characterization of the morphological and functional features of 2D and 3D thyroid culture models. Consistent with previous reports, thyrocytes in a conventional 2D monolayer were able to reproduce some aspects of native thyroid function such as TSH-dependent gene expression and TG production. However, the 2D culture format was clearly deficient for all integral components needed for thyroid hormonogenesis. Adaptation to a 3D hydrogel culture model using medium optimized for human thyrocytes restored production of iodothyronine hormones for up to 20 days in a stable, long-term, *in vitro* culture model. Moreover, by establishing the 3D microtissue model in a 96-well culture format, inhibition of TH synthesis could be reproducibly interrogated using a reference set of known TDCs to directly assess the efficacy and potency of TH disruption in a concentration-dependent manner.

Unlike many immortalized cell lines, primary cells often have fastidious requirements for optimal growth in cell culture. One of the most commonly used medium formulation for primary thyroid cell culture is based on the composition initially optimized for FRTL rat thyrocytes (Ambesi-Impiombato *et al.*, 1980). The formulation is comprised of Ham's F-12 base medium supplemented with calf serum and 6 additives: insulin, hydrocortisone, transferrin, glycl-L-histidyl-L-lysine acetate, somatostatin, and TSH. Both the choice of hormone components and concentrations has been deemed suboptimal for human thyroid cell culture. A recent publication investigating the utility of h7H medium identified a formulation with additives adjusted to the relative normal homeostatic serum ranges in humans (Bravo

et al., 2013). In addition to a mixture of serum, it contains hormones, transferrin, iodine, trace elements, antioxidants, and metabolites optimized for human cells. This base formulation was adequate for maintaining and expanding cells in 2D culture. However, for optimal performance, TSH levels greater than the specified concentration of 0.04 mU/mL (Bravo *et al.*, 2013) were necessary to maximize cellular responses, particularly in the 3D culture format. Effects on gene expression, TG protein production, and TH output were most consistent when cultures were maintained at markedly higher levels of 1 mU/ml TSH, so this concentration in h7H medium was considered optimal for maximizing the dynamic range in the 3D microtissue assay. Another important consideration in the assay medium was the substitution of normal sera for charcoal-stripped sera at the 8–10 day transition point (Figure 1B). Fetal bovine and newborn calf sera are rich in TH and would interfere with measurements for TH levels when conducting the assay. The transition to hormone-depleted CS-FBS enabled clear determination of iodotyrosine and TH accumulation, not present in the 2D model, that could be directly attributed to hormonogenesis from the human microtissues (Figure 6). It is unclear if the entire assay could be performed in CS-FBS to circumvent the transition period, or if TH accumulates earlier than 10 days, so future work to optimize the assay would focus on these parameters.

The ECM plays an important role in modifying cellular function (Humphrey *et al.*, 2014). In the case of thyrocytes, standard tissue culture plates can result in abnormal polarization and loss of a differentiated phenotype. The major basement membrane constituents naturally synthesized and secreted by porcine thyrocytes are collagen type I, III, and IV (Wadeleux *et al.*, 1985). Development of *in vitro* follicles from monolayer cultures embedded in collagen type I was initially reported for porcine (Chambard *et al.*, 1981) and rat (Garbi *et al.*, 1984) thyrocytes. Human follicles have been developed in a similar manner where reorganization of cells seeded into a collagen matrix revealed follicular structures with increased TSH-dependent cAMP induction, as well as accumulation of free T4 and T3 in the media supernatant (Massart *et al.*, 1988; Thomas-Morvan *et al.*, 1988). More recently, Matrigel, a mixed ECM composition of laminin, collagen, and entactin, has been utilized to stimulate follicle formation from primary murine thyrocytes, as well as the rat FRTL thyrocyte cell line (Koumarianou *et al.*, 2016). The collective evidence suggested a 3D culture system comprised of a native ECM composed predominantly of collagen would be suitable for model development of human 3D microtissues. Indeed, inclusion of a thick Matrigel basement membrane provided an adequate substrate for human thyrocytes to migrate and self-assemble into microtissues (Figure 3A). Over time, the microtissues matured to form follicular structures that attained lumen-like cavities that were stable for the duration of the culture (Figure 3B). Coinciding with consistent output of TH, the morphology suggests the microtissues had matured to a functional state that could be probed for compound disrupting effects.

TSH had a notable impact on expression of several genes in the TH synthesis pathway between the culture formats. For instance, maximal expression of several TH-related genes was observed when cultures were stimulated at a TSH concentration of 1 mU/ml (Figure 4). Most notably, the expression of SLC5A5 (NIS) exhibited expression almost exclusively in the 3D microtissue model when TSH was supplemented in the medium. A similar observation has been made in reconstituted thyroid follicles of porcine thyrocytes where both *NIS* transcript and protein levels were only detected when cells had undergone histotypic morphogenesis in a 3D culture model stimulated by TSH (Bernier-Valentin *et al.*, 2006). In humans thyrocytes, conditions stimulating follicle formation with concurrent TSH exposure significantly increased iodide uptake despite no change observed in *NIS* transcript or protein levels (Kogai *et al.*, 2000). *NIS* expression appears late in thyroid development and is a limiting step toward full thyroid function in the human fetus (Szinnai *et al.*, 2007), so it is reasonable to conclude that the 3D microtissues represent a more mature state of differentiation and function by day 8 of culture. An additional gene, Dual Oxidase Maturation Factor 2 (*DUOXA2*), is required for the proper subcellular localization and maturation of Dual Oxidase 2 (*DUOX2*), an apical membrane protein important for TPO-catalyzed oxidation of iodide in the follicular lumen (Grasberger and Refetoff, 2006). Like *NIS*, *DUOXA2* expression was predominantly observed in the 3D microtissue model. Together, the results suggest the absence of TH observed in 2D monolayer cultures (Figure 6) may be, in part, due to insufficient iodide uptake and organification.

Formation of nascent TH is a multi-step process that begins with concentrating serum iodide in thyrocytes via basal membrane transporters. A coordinated reaction of iodide oxidation and organification is catalyzed by thyroperoxidase and dual oxidases present along the apical membrane border of the lumen where iodine is subsequently conjugated to tyrosyl residues present within TG protein to form iodotyrosines MIT and DIT (Kopp and Solis-S, 2009). This process of iodide organification is a critical mechanism for iodine storage within the follicular lumen. Interestingly, both MIT and DIT were present above background levels in conditioned culture medium only in 3D cultures stimulated with TSH (Figure 6). Although DIT is generally considered to be the major product, it was detected in considerably lower levels than MIT, with mean concentrations 24- and 22-fold higher at 1 and 5 mU/ml TSH, respectively, across all time points (Supplementary Table 4). The coupling of iodotyrosine residues results in DIT–DIT and DIT–MIT containing peptides that will undergo hydrolysis to the TH products T4 and T3, respectively (Kopp and Solis-S, 2009). Like the iodotyrosine products, a similar trend was observed for T4 and T3, where the presence of these hormones above background in the culture medium was restricted to the 3D model in the TSH-treatment groups (Figure 6). Daily thyroid-derived production, as a function of body surface area, for T4 is 56.2 μg/day/m^2 and for T3 is 3.3 μg/day/m^2, yielding a T4/T3 ratio of 16.8 (Pilo *et al.*, 1990). In the 3D microtissue model, T4 was present at a mean T4:T3 ratio of 2.6- and 2.4-fold at 1 and 5 mU/ml TSH. Based on these observations, the human microtissue model appears to synthesize T4 and T3 in a manner that trends toward the *in vivo* stoichiometric production ratio but is considerably lower than expected for reasons that are not clear. Additional characterization of TH regulation by thyroid-specific deiodinases (eg IYD, DIO1) in the 3D culture model may provide additional insight into this variability. Deiodinase enzymes have been identified as potentially relevant targets in HTS assays for TH disruption by environmental chemicals (Hornung *et al.*, 2018; Olker *et al.*, 2019), so evaluation of activity within this culture model would be necessary to determine the utility in orthogonal screening of these putative TDCs. Despite some donor-dependent variability in TH analyte concentrations, T4 secretion over the 10–20 sampling period was fairly stable, pointing to the utility of the 3D microtissue model for long-term culture monitoring of T4 biosynthesis.

Adverse outcome pathways (AOPs) provide a framework for understanding the relationship of MIEs to adverse toxicity outcomes based on biological relationships of mechanistic, measurable events (Ankley *et al.*, 2010). Thyroid-related AOPs mapping the MIE relationship of TSHR, TPO, and NIS to toxicity-mediated thyroid dysgenesis, reduction in serum thyroxine (T4)

levels, and altered neurodevelopmental outcome have been proposed (EPA, 2017; Miller *et al.*, 2009; Perkins *et al.*, 2013). Here, several reference chemicals for thyroid-specific targets were evaluated in an optimized 3D microtissue culture model. The thionamides methimazole and 6-propyl-2-thiouracil inhibit the TPO enzyme in humans and are clinically approved for use in hyperthyroid patients (Emiliano *et al.*, 2010). The relative potency of T4 inhibition (Table 4) for methimazole in the 3D microtissue model (IC_{50}: 0.129 μM, LEC: 1 μM) was in the range previously reported for TPO inhibition assays from rat (IC_{50}: 0.025–2.22 μM; Paul *et al.*, 2013, 2014), porcine (IC_{50}: 0.67–1 μM; Hornung *et al.*, 2015; Paul *et al.*, 2013; Tietge *et al.*, 2013), and human (IC_{50}: 0.8–2.7 μM; Jomaa *et al.*, 2015; Nagasaka and Hidaka, 1976) microsomes, and considerably more potent than TPO inhibition observed in *ex vivo* models of rat thyroid (LEC 10 μM; Vickers *et al.*, 2012), porcine follicles (LOEL 100 μM; Sugawara *et al.*, 1999), or human organotypic culture slices (LOEL 10 μM; Vickers *et al.*, 2012). The potency was also considerably higher than in a *Xenopus laevis* thyroid gland explant model of T4 inhibition (IC_{50}: 10–13 μM; Hornung *et al.*, 2015, 2010). As expected, 6-propyl-2-thiouracil potency (IC_{50}: 0.172 μM, LEC: 1 μM)) was less than methimazole and more similar to ranges observed in rat (IC_{50}: 0.12–1.28 μM; Paul *et al.*, 2013, 2014), than porcine (IC_{50}: 10.7–18.4 μM; Jomaa *et al.*, 2015; Paul *et al.*, 2013), or human (IC_{50}: 2–35.2 μM; Jomaa *et al.*, 2015; Nagasaka and Hidaka, 1976) TPO assays. Likewise, inhibition of T4 synthesis was more effective than a *X. laevis* explant model (IC_{50}: 8.6 μM; Hornung *et al.*, 2010). For NIS inhibition, sodium perchlorate reduced T4 output (IC_{50}: 3.233 μM, LEC: 10 μM) with a potency that was only slightly less than NIS inhibition evaluated in engineered hNIS-HEK293(T) cells (IC_{50}: 0.866–1 μM; Hallinger *et al.*, 2017; Lecat-Guillet *et al.*, 2008) and immortalized rat FRTL-5 thyrocytes (IC_{50}: 0.1–0.2 μM; Lecat-Guillet *et al.*, 2008; Waltz *et al.*, 2010). Lastly, VA-K-14 (IC_{50}: 5.614 μM, LEC: 10 μM) exhibited comparable potency as *in vitro* assays for hTSHR measuring inhibition of cAMP induction and downstream signaling (IC_{50}: 12.3 μM; Latif *et al.*, 2016). The similar potencies observed across these 3 MIEs in the 3D microtissue assay to other target-specific HTS assays highlights the sensitivity in detecting target-level perturbations but suggests there may be greater value in orthogonal confirmation of molecular effect to TH synthesis, rather than extrapolation of tissue-level potency. Although the microtissue assay does not take into account serum hormone protein binding or peripheral tissue uptake and metabolism, the effect on relative T4 levels in the medium may provide some context to decreases in serum T4 levels measured in animal models. Transient decreases in serum T4 of 28–50% during critical periods of fetal development have been noted to produce adverse effects on brain development in rodents (Auso *et al.*, 2004; Crofton, 2004; Gilbert and Sui, 2008; Sharlin *et al.*, 2008) and each of the reference compounds in this study produced decreases in the range of 28–51%, supporting the likelihood of inducing an adverse *in vivo* outcome. Additional screening with other prioritized test compounds is necessary to further evaluate the predictive utility of the assay.

Continuing in the framework of the EDSP Comprehensive Management Plan (EPA, 2014), there have been ongoing efforts to address needs in thyroid screening (EPA, 2017) with development and application of thyroid-related HTS assays. Similar efforts have been made within the OECD and member countries in the European Union with identification of *in vitro* and *ex vivo* test methods (OECD, 2017), as well as potential gaps that need to be filled (Kortenkamp *et al.*, 2017), to appropriately identify TDCs. Although useful for prioritization, it is less clear if chemicals identified by HTS assays alter thyroid function *in vivo* or elicit adverse outcomes. Key components to interpreting these data will rely on understanding the efficacy, potency, statistical uncertainty, and biological relevance of TDCs identified across the high-throughput platforms. Here, a 3D culture model of the human thyroid that recapitulates TH biosynthesis provides initial evidence of an *in vitro* assay that can bridge high-throughput data to apical effects in the human thyroid. Through careful systematic review of bioactive chemicals from HTS assays, chemicals deemed to pose the greatest risk to thyroid function can be screened for orthogonal evaluation. Generated data may enable more direct interpretation of molecular perturbation effects on TH production. Since alterations in serum TH levels are one of the most common biomarkers in EDSP guideline studies, this 3D microtissue assay may provide an alternative to more expensive and time-intensive Tier 1 and 2 *in vivo* thyroid tests (rat pubertal, amphibian metamorphosis assay, rat extended one-generation reproductive toxicity study, and larval amphibian growth and development assay), ultimately reducing the number of animal tests required while providing some context for evaluating adverse thyroid-related outcomes in human populations for regulatory decision-making.

SUPPLEMENTARY DATA

Supplementary data are available at *Toxicological Sciences* online.

DECLARATION OF CONFLICTING INTERESTS

V.Y.S. and E.L.L. are currently employed by LifeNet Health. There are no other conflicts to declare.

ACKNOWLEDGEMENTS

The authors thank Dr Steve Simmons, Dr Mary Gilbert, and Dr Kevin Crofton for providing critical comments and technical review of this article.

FUNDING

U.S. Environmental Protection Agency.

REFERENCES

Ambesi-Impiombato, F. S., and Villone, G. (1987). The FRTL-5 thyroid cell strain as a model for studies on thyroid cell growth. *Acta Endocrinol. Suppl.* **281**, 242–245.

Ambesi-Impiombato, F. S., Parks, L. A., and Coon, H. G. (1980). Culture of hormone-dependent functional epithelial cells from rat thyroids. *Proc. Natl. Acad. Sci. U S A* **77**, 3455–3459.

Ankley, G. T., Bennett, R. S., Erickson, R. J., Hoff, D. J., Hornung, M. W., Johnson, R. D., Mount, D. R., Nichols, J. W., Russom, C. L., Schmieder, P. K., *et al.* (2010). Adverse outcome pathways: A conceptual framework to support ecotoxicology research and risk assessment. *Environ. Toxicol. Chem.* **29**, 730–741.

Aouani, A., Hovsepian, S., and Fayet, G. (1987). cAMP dependent and independent regulation of thyroglobulin synthesis by two clones of the OVNIS 6H thyroid cell line. *Mol. Cell. Endocrinol.* **52**, 151–160.

Asmis, L. M., Kaempf, J., Von Gruenigen, C., Kimura, E. T., Wagner, H. E., and Studer, H. (1996). Acquired and naturally occurring resistance of thyroid follicular cells to the growth inhibitory action of transforming growth factor-beta 1 (TGF-beta 1). *J. Endocrinol.* **149**, 485–496.

Auso, E., Lavado-Autric, R., Cuevas, E., Del Rey, F. E., Morreale De Escobar, G., and Berbel. P. (2004). A moderate and transient deficiency of maternal thyroid function at the beginning of fetal neocorticogenesis alters neuronal migration. *Endocrinology* **145**, 4037–4047.

Bassett, J. H., and Williams, G. R. (2016). Role of thyroid hormones in skeletal development and bone maintenance. *Endocr. Rev.* **37**, 135–187.

Bernier-Valentin, F., Trouttet-Masson, S., Rabilloud, R., Selmi-Ruby, S., and Rousset, B. (2006). Three-dimensional organization of thyroid cells into follicle structures is a pivotal factor in the control of sodium/iodide symporter expression. *Endocrinology* **147**, 2035–2042.

Bianco, A. C., Anderson, G., Forrest, D., Galton, V. A., Gereben, B., Kim, B. W., Kopp, P. A., Liao, X. H., Obregon, M. J., Peeters, R. P., *et al.* (2014). American Thyroid Association Guide to investigating thyroid hormone economy and action in rodent and cell models. *Thyroid* **24**, 88–168.

Boas, M., Feldt-Rasmussen, U., Skakkebæk, N. E., and Main, K. M. (2006). Environmental chemicals and thyroid function. *Eur. J. Endocrinol.* **154**, 599–611.

Brandi, M. L., Rotella, C. M., Mavilia, C., Franceschelli, F., Tanini, A., and Toccafondi, R. (1987). Insulin stimulates cell growth of a new strain of differentiated rat thyroid cells. *Mol. Cell. Endocrinol.* **54**, 91–103.

Bravo, S. B., Garcia-Rendueles, M. E. R., Garcia-Rendueles, A. R., Rodrigues, J. S., Perez-Romero, S., Garcia-Lavandeira, M., Suarez-Fariña, M., Barreiro, F., Czarnocka, B., Senra, A., *et al.* (2013). Humanized medium (h7H) allows long-term primary follicular thyroid cultures from human normal thyroid, benign neoplasm, and cancer. *J. Clin. Endocrinol. Metab.* **98**, 2431–2441.

Brent, G. A. (2012). Mechanisms of thyroid hormone action. *J. Clin. Invest.* **122**, 3035–3043.

Brucker-Davis, F. (1998). Effects of environmental synthetic chemicals on thyroid function. *Thyroid: official Journal of the American Thyroid Association* **8**, 827–856. doi: 10.1089/thy.1998.8.827

Chambard, M., Gabrion, J., and Mauchamp, J. (1981). Influence of collagen gel on the orientation of epithelial cell polarity: Follicle formation from isolated thyroid cells and from preformed monolayers. *J. Cell Biol.* **91**, 157–166.

Citterio, C. E., Targovnik, H. M., and Arvan, P. (2019). The role of thyroglobulin in thyroid hormonogenesis. *Nat. Rev. Endocrinol.* **15**, 323–338.

Colin, I. M., Denef, J. F., Lengele, B., Many, M. C., and Gerard, A. C. (2013). Recent insights into the cell biology of thyroid angiofollicular units. *Endocr. Rev.* **34**, 209–238.

Coppa, A., Mincione, G., Mammarella, S., Ranieri, A., and Colletta, G. (1995). Epithelial rat thyroid cell clones, escaping from transforming growth factor beta negative growth control, are still inhibited by this factor in the ability to trap iodide. *Cell Growth Differ.* **6**, 281–290.

Crofton, K. M. (2004). Developmental disruption of thyroid hormone: Correlations with hearing dysfunction in rats. *Risk Anal.* **24**, 1665–1671.

Davies, T. F., Yang, C., and Platzer, M. (1987). Cloning the Fisher rat thyroid cell line (FRTL-5): variability in clonal growth and 3′,5′-cyclic adenosine monophosphate response to thyrotropin. *Endocrinology* **121**, 78–83.

De Benoist, B., Andersson, M., Egli, I., Takkouche, B., Allen, H. (2004). Iodine status worldwide. WHO global database on iodine deficiency. World Health Organization, Geneva.

DeVito, M., Biegel, L., Brouwer, A., Brown, S., Brucker-Davis, F., Cheek, A. O., Christensen, R., Colborn, T., Cooke, P., Crissman, J., *et al.* (1999). Screening methods for thyroid hormone disruptors. *Environ. Health Perspect.* **107**, 407–415.

Eggo, M. C., Bachrach, L. K., Fayet, G., Errick, J., Kudlow, J. E., Cohen, M. F., and Burrow, G. N. (1984). The effects of growth factors and serum on DNA synthesis and differentiation in thyroid cells in culture. *Mol. Cell. Endocrinol.* **38**, 141–150.

Eggo, M. C., King, W. J., Black, E. G., and Sheppard, M. C. (1996). Functional human thyroid cells and their insulin-like growth factor-binding proteins: Regulation by thyrotropin, cyclic 3′,5′ adenosine monophosphate, and growth factors. *J. Clin. Endocrinol. Metab.* **81**, 3056–3062.

Emiliano, A. B., Governale, L., Parks, M., and Cooper, D. S. (2010). Shifts in propylthiouracil and methimazole prescribing practices: Antithyroid drug use in the United States from 1991 to 2008. *J. Clin. Endocrinol. Metab.* **95**, 2227–2233.

Ericson, L. E., and Nilsson, M. (1996). Effects of insulin-like growth factor I on growth, epithelial barrier and iodide transport in polarized pig thyrocyte monolayers. *Eur. J. Endocrinol.* **135**, 118–127.

Fagerberg, L. (2014). Analysis of the human tissue-specific expression by genome-wide integration of transcriptomics and antibody-based proteomics. *Mol. Cell. Proteomics* **13**, 397–406.

Forhead, A. J., and Fowden, A. L. (2014). Thyroid hormones in fetal growth and prepartum maturation. *J. Endocrinol.* **221**, R87–R103.

Fusco, A., Berlingieri, M. T., Di Fiore, P. P., Portella, G., Grieco, M., and Vecchio, G. (1987). One- and two-step transformations of rat thyroid epithelial cells by retroviral oncogenes. *Mol. Cell. Biol.* **7**, 3365–3370.

Garbi, C., Nitsch, L., and Wollman, S. H. (1984). Embedding in a collagen gel stabilizes the polarity of epithelial cells in thyroid follicles in suspension culture. *Exp. Cell Res.* **151**, 458–465.

Garbi, C., Tacchetti, C., and Wollman, S. H. (1986). Change of inverted thyroid follicle into a spheroid after embedding in a collagen gel. *Exp. Cell Res.* **163**, 63–77.

Gerard, C. M., Roger, P. P., and Dumont, J. E. (1989). Thyroglobulin gene expression as a differentiation marker in primary cultures of calf thyroid cells. *Mol. Cell. Endocrinol.* **61**, 23–35.

Gilbert, M. E., and Sui, L. (2008). Developmental exposure to perchlorate alters synaptic transmission in hippocampus of the adult rat. *Environ. Health Perspect.* **116**, 752–760.

Gothe, S., Wang, Z., Ng, L., Kindblom, J. M., Barros, A. C., Ohlsson, C., Vennström, B., and Forrest, D. (1999). Mice devoid of all known thyroid hormone receptors are viable but exhibit disorders of the pituitary-thyroid axis, growth, and bone maturation. *Genes Dev.* **13**, 1329–1341.

Grasberger, H., and Refetoff, S. (2006). Identification of the maturation factor for dual oxidase. Evolution of an eukaryotic operon equivalent. *J. Biol. Chem.* **281**, 18269–18272.

Hallinger, D. R., Murr, A. S., Buckalew, A. R., Simmons, S. O., Stoker, T. E., and Laws, S. C. (2017). Development of a screening approach to detect thyroid disrupting chemicals that inhibit the human sodium iodide symporter (NIS). *Toxicol. In Vitro* **40**, 66–78.

Hornung, M. W., Degitz, S. J., Korte, L. M., Olson, J. M., Kosian, P. A., Linnum, A. L., and Tietge, J. E. (2010). Inhibition of thyroid hormone release from cultured amphibian thyroid glands by methimazole, 6-propylthiouracil, and perchlorate. *Toxicol. Sci.* **118**, 42–51.

Hornung, M. W., Korte, J. J., Olker, J. H., Denny, J. S., Knutsen, C., Hartig, P. C., Cardon, M. C., and Degitz, S. J. (2018). Screening the ToxCast phase 1 chemical library for inhibition of deiodinase type 1 activity. *Toxicol. Sci.* **162**, 570–581.

Hornung, M. W., Kosian, P. A., Haselman, J. T., Korte, J. J., Challis, K., Macherla, C., Nevalainen, E., and Degitz, S. J. (2015). In vitro, ex vivo, and in vivo determination of thyroid hormone modulating activity of benzothiazoles. *Toxicol. Sci.* **146**, 254–264.

Huber, G., Derwahl, M., Kaempf, J., Peter, H.-J., Gerber, H., and Studer, H. (1990). Generation of intercellular heterogeneity of growth and function in cloned rat thyroid cells (FRTL-5). *Endocrinology* **126**, 1639–1645.

Humphrey, J. D., Dufresne, E. R., and Schwartz, M. A. (2014). Mechanotransduction and extracellular matrix homeostasis. *Nat. Rev. Mol. Cell Biol.* **15**, 802–812.

Jomaa, B., de Haan. L. H.Peijnenburg, A. A., Bovee, T. F., Aarts, J. M., and Rietjens, I. M. (2015). Simple and rapid in vitro assay for detecting human thyroid peroxidase disruption. *ALTEX* **32**, 191–200.

Kogai, T., Curcio, F., Hyman, S., Cornford, E. M., Brent, G. A., and Hershman, J. M. (2000). Induction of follicle formation in long-term cultured normal human thyroid cells treated with thyrotropin stimulates iodide uptake but not sodium/iodide symporter messenger RNA and protein expression. *J. Endocrinol.* **167**, 125–135.

Kohrle, J. (1999). Local activation and inactivation of thyroid hormones: the deiodinase family. *Mol. Cell. Endocrinol.* **151**, 103–119.

Koibuchi, N. (2018). Molecular Mechanisms of Thyroid Hormone Synthesis and Secretion. In *Principles of Endocrinology and Hormone Action* (A. Belfiore and D. LeRoith, Eds.), pp. 73–81. Springer International Publishing.

Kopp, P., and Solis-S, J. C. (2009). Thyroid Hormone Synthesis. In *Clinical Management of Thyroid Disease* (F. E. Wondisford and S. Radovick, 19–41. W.B. Saunders, Philadelphia. PA.

Kortenkamp, A., Martin, O., Baynes, A., Silva, E., Axelstad, M., Hass, U. (2017). *Supporting the Organisation of a Workshop on Thyroid Disruption — Final Report*. DG Environment, European Commission.

Koumarianou, P., Gomez-Lopez, G., and Santisteban, P. (2016). Pax8 controls thyroid follicular polarity through Cadherin-16. *J. Cell Sci.* **130**, 219–231.

Kraiem, Z., Sadeh, O., and Yosef, M. (1991). Iodide uptake and organification, tri-iodothyronine secretion, cyclic AMP accumulation and cell proliferation in an optimized system of human thyroid follicles cultured in collagen gel suspended in serum-free medium. *J. Endocrinol.* **131**, 499–506.

Kusunoki, T., Nishida, S., Koezuka, M., Murata, K., and Tomura, T. (1995). Productivity of thyroglobulin and thyroid hormone on human thyroid cell in collagen gel culture. *Auris Nasus Larynx* **22**, 120–127.

Kusunoki, T., Nishida, S., Koezuka, M., Murata, K., and Tomura, T. (2001). Morphological and functional differentiation of human thyroid cells in collagen gel culture. *Auris Nasus Larynx* **28**, 333–338.

Latif, R., Realubit, R. B., Karan, C., Mezei, M., and Davies, T. F. (2016). TSH receptor signaling abrogation by a novel small molecule. *Front. Endocrinol.* **7**, 130.

Lecat-Guillet, N., Merer, G., Lopez, R., Pourcher, T., Rousseau, B., and Ambroise, Y. (2008). Small-molecule inhibitors of sodium iodide symporter function. *Chembiochem* **9**, 889–895.

Lemoine, N. R., Mayall, E. S., Jones, T., Sheer, D., McDermid, S., Kendall-Taylor, P., and Wynford-Thomas, D. (1989). Characterisation of human thyroid epithelial cells immortalised in vitro by simian virus 40 DNA transfection. *Br. J. Cancer* **60**, 897–903.

Li, M., Iismaa, S. E., Naqvi, N., Nicks, A., Husain, A., and Graham, R. M. (2014). Thyroid hormone action in postnatal heart development. *Stem Cell Res.* **13**, 582–591.

Lindsey, R. C., Aghajanian, P., and Mohan, S. (2018). Thyroid hormone signaling in the development of the endochondral skeleton. *Vitam. Horm.* **106**, 351–381.

Lissitzky, S., Fayet, G., Giraud, A., Vernier, B., and Torresani, J. (1971). Thyrotrophin-induced aggregation and reorganization into follicles of isolated porcine-thyroid cells. 1. Mechanism of action of thyrotrophin and metabolic properties. *Eur. J. Biochem.* **24**, 88–99.

Liu, Y. Y., and Brent, G. A. (2018). Thyroid hormone and the brain: Mechanisms of action in development and role in protection and promotion of recovery after brain injury. *Pharmacol. Ther.* **186**, 176–185.

Luna, L. G., Coady, K., McFadden, J. R., Markham, D. A., and Bartels, M. J. (2013). Quantification of total thyroxine in plasma from *Xenopus laevis*. *J. Anal. Toxicol.* **37**, 326–336.

Massart, C., Hody, B., Condé, D., Leclech, G., Edan, G., and Nicol, M. (1988). Functional properties of human thyroid follicles cultured within collagen gel. *Mol. Cell. Endocrinol.* **56**, 227–234.

Mauchamp, J., Margotat, A., Chambard, M., Charrier, B., Remy, L., and Michel-Bechet, M. (1979). Polarity of three-dimensional structures derived from isolated hog thyroid cells in primary culture. *Cell Tissue Res.* **204**, 417–430.

McAninch, E. A., and Bianco, A. C. (2014). Thyroid hormone signaling in energy homeostasis and energy metabolism. *Ann. N. Y. Acad. Sci.* **1311**, 77–87.

Miller, M. D., Crofton, K. M., Rice, D. C., and Zoeller, R. T. (2009). Thyroid-disrupting chemicals: Interpreting upstream biomarkers of adverse outcomes. *Environ. Health Perspect.* **117**, 1033–1041.

Mullur, R., Liu, Y. Y., and Brent, G. A. (2014). Thyroid hormone regulation of metabolism. *Physiol. Rev.* **94**, 355–382.

Murk, A. J., Rijntjes, E., Blaauboer, B. J., Clewell, R., Crofton, K. M., Dingemans, M. M. L., David Furlow, J., Kavlock, R., Köhrle, J., Opitz, R., *et al.* (2013). Mechanism-based testing strategy using in vitro approaches for identification of thyroid hormone disrupting chemicals. *Toxicol. In Vitro* **27**, 1320–1346.

Nagasaka, A., and Hidaka, H. (1976). Effect of antithyroid agents 6-propyl-2-thiouracil and 1-mehtyl-2-mercaptoimidazole on human thyroid iodine peroxidase. *J. Clin. Endocrinol. Metab.* **43**, 152–158.

Nilsson, M., and Fagman, H. (2017). Development of the thyroid gland. *Development* **144**, 2123–2140.

OECD (2017), New Scoping Document on in vitro and ex vivo Assays for the Identification of Modulators of Thyroid Hormone Signalling, OECD Series on Testing and Assessment, No. 207, OECD Publishing, Paris, https://doi.org/10.1787/9789264274716-en.

Olker, J. H., Korte, J. J., Denny, J. S., Hartig, P. C., Cardon, M. C., Knutsen, C. N., Kent, P. M., Christensen, J. P., Degitz, S. J., Hornung, M. W., *et al.* (2019). Screening the ToxCast phase 1, phase 2, and e1k chemical libraries for inhibitors of iodothyronine deiodinases. *Toxicol. Sci.* **168**, 430–442.

Paul Friedman, K., Watt, E. D., Hornung, M. W., Hedge, J. M., Judson, R. S., Crofton, K. M., Houck, K. A., and Simmons, S. O. (2016). Tiered high-throughput screening approach to identify thyroperoxidase inhibitors within the ToxCast phase I and II chemical libraries. *Toxicol. Sci.* **151**, 160–180.

Paul, K. B., Hedge, J. M., Macherla, C., Filer, D. L., Burgess, E., Simmons, S. O., Crofton, K. M., and Hornung, M. W. (2013). Cross-species analysis of thyroperoxidase inhibition by xenobiotics demonstrates conservation of response between pig and rat. *Toxicology* **312**, 97–107.

Paul, K. B., Hedge, J. M., Rotroff, D. M., Hornung, M. W., Crofton, K. M., and Simmons, S. O. (2014). Development of a

thyroperoxidase inhibition assay for high-throughput screening. *Chem. Res. Toxicol.* **27**, 387–399.

Perkins, E. J., Ankley, G. T., Crofton, K. M., Garcia-Reyero, N., LaLone, C. A., Johnson, M. S., Tietge, J. E., and Villeneuve, D. L. (2013). Current perspectives on the use of alternative species in human health and ecological hazard assessments. *Environ. Health Perspect.* **121**, 1002–1010.

Pilo, A., Iervasi, G., Vitek, F., Ferdeghini, M., Cazzuola, F., and Bianchi R. (1990). Thyroidal and peripheral production of 3,5,3′-triiodothyronine in humans by multicompartmental analysis. *Am. J. Physiol.* **258**, E715–E726.

Postiglione, M. P., Parlato, R., Rodriguez-Mallon, A., Rosica, A., Mithbaokar, P., Maresca, M., Marians, R. C., Davies, T. F., Zannini, M. S., De Felice, M., *et al.* (2002). Role of the thyroid-stimulating hormone receptor signaling in development and differentiation of the thyroid gland. *Proc. Natl. Acad. Sci. U S A* **99**, 15462–15467.

Rapoport, B. (1976). Dog thyroid cells in monolayer tissue culture: Adenosine 3′,5′-cyclic monophosphate response to thyrotropic hormone. *Endocrinology* **98**, 1189–1197.

Roger, P. P., Christophe, D., Dumont, J. E., and Pirson, I. (1997). The dog thyroid primary culture system: a model of the regulation of function, growth and differentiation expression by cAMP and other well-defined signaling cascades. *Eur. J. Endocrinol.* **137**, 579–598.

Roger, P., Taton, M., Van Sande, J., and Dumont, J. E. (1988). Mitogenic effects of thyrotropin and adenosine 3′,5′-monophosphate in differentiated normal human thyroid cells in vitro. *J. Clin. Endocrinol. Metab.* **66**, 1158–1165.

Schmutzler, C., Gotthardt, I., Hofmann, P. J., Radovic, B., Kovacs, G., Stemmler, L., Nobis, I., Bacinski, A., Mentrup, B., Ambrugger, P., *et al.* (2007). Endocrine disruptors and the thyroid gland—A combined in vitro and in vivo analysis of potential new biomarkers. *Environ. Health Perspect.* **115(Suppl. 1)**, 77–83.

Sharlin, D. S., Tighe, D., Gilbert, M. E., and Zoeller, R. T. (2008). The balance between oligodendrocyte and astrocyte production in major white matter tracts is linearly related to serum total thyroxine. *Endocrinology* **149**, 2527–2536.

Sugawara, M., Sugawara, Y., and Wen, K. (1999). Methimazole and propylthiouracil increase cellular thyroid peroxidase activity and thyroid peroxidase mRNA in cultured porcine thyroid follicles. *Thyroid* **9**, 513–518.

Szinnai, G. (2014). Genetics of normal and abnormal thyroid development in humans. *Best Pract. Res. Clin. Endocrinol. Metab.* **28**, 133–150.

Szinnai, G., Lacroix, L., Carré, A., Guimiot, F., Talbot, M., Martinovic, J., Delezoide, A.-L., Vekemans, M., Michiels, S., Caillou, B., *et al.* (2007). Sodium/iodide symporter (NIS) gene expression is the limiting step for the onset of thyroid function in the human fetus. *J. Clin. Endocrinol. Metab.* **92**, 70–76.

Thomas, R. S., Bahadori, T., Buckley, T. J., Cowden, J., Deisenroth, C., Dionisio, K. L., Frithsen, J. B., Grulke, C. M., Gwinn, M. R., Harrill, J. A., *et al.* (2019). The next generation blueprint of computational toxicology at the U.S. Environmental Protection Agency. *Toxicol. Sci.* **169**, 317.

Thomas-Morvan, C., Caillou, B., Schlumberger, M., and Fragu, P. (1988). Morphological and functional differentiation of human thyroid cells in collagen gel culture. *Biol. Cell* **62**, 247–254.

Tietge, J. E., Degitz, S. J., Haselman, J. T., Butterworth, B. C., Korte, J. J., Kosian, P. A., Lindberg-Livingston, A. J., Burgess, E. M., Blackshear, P. E., Hornung, M. W., *et al.* (2013). Inhibition of the thyroid hormone pathway in *Xenopus laevis* by 2-mercaptobenzothiazole. *Aquat. Toxicol.* **126**, 128–136.

Titus, S., Neumann, S., Zheng, W., Southall, N., Michael, S., Klumpp, C., Yasgar, A., Shinn, P., Thomas, C. J., Inglese, J. *et al.* (2008). Quantitative high-throughput screening using a live-cell cAMP assay identifies small-molecule agonists of the TSH receptor. *J. Biomol. Screen.* **13**, 120–127.

Toda, S., Yonernitsu, N., Hikichi, Y., Sugihara, H., and Koike, N. (1992). Differentiation of human thyroid follicle cells from normal subjects and Basedow's disease in three-dimensional collagen gel culture. *Pathol. Res. Pract.* **188**, 874–882.

United States Environmental Protection Agency (EPA). (2014). *Endocrine Disruptor Screening Program Comprehensive Management Plan*. https://www.epa.gov/sites/production/files/2015-08/documents/edsp_comprehesive_management_plan_021414_f.pdf

United States Environmental Protection Agency (EPA). (2017). *Continuing Development of Alternative High-Throughput Screens to Determine Endocrine Disruption, Focusing on Androgen Receptor, Steroidogenesis, and Thyroid Pathways*. FIFRA SAP, November 28–30. https://www.epa.gov/sites/production/files/2017-09/documents/2017_edsp_white_paper_public.pdf

van Staveren, W. C. G., Solís, D. W., Delys, L., Duprez, L., Andry, G., Franc, B., Thomas, G., Libert, F., Dumont, J. E., Detours, V., *et al.* (2007). Human thyroid tumor cell lines derived from different tumor types present a common dedifferentiated phenotype. *Cancer Res.* **67**, 8113–8120.

Vickers, A. E. M., Heale, J., Sinclair, J. R., Morris, S., Rowe, J. M., and Fisher, R. L. (2012). Thyroid organotypic rat and human cultures used to investigate drug effects on thyroid function, hormone synthesis and release pathways. *Toxicol. Appl. Pharmacol.* **260**, 81–88.

Wadeleux, P., Nusgens, B., Foidart, J. M., Lapiere, C., and Winand, R. (1985). Synthesis of basement membrane components by differentiated thyroid cells. *Biochim. Biophys. Acta* **846**, 257–264.

Waltz, F., Pillette, L., and Ambroise, Y. (2010). A nonradioactive iodide uptake assay for sodium iodide symporter function. *Anal. Biochem.* **396**, 91–95.

Wang, J., Hallinger, D. R., Murr, A. S., Buckalew, A. R., Simmons, S. O., Laws, S. C., Stoker, T. E. (2018). High-throughput screening and quantitative chemical ranking for sodium-iodide symporter inhibitors in ToxCast phase I chemical library. *Environ. Sci. Technol.* **52**, 5417–5426.

Wang, J., Hallinger, D. R., Murr, A. S., Buckalew, A. R., Lougee, R. R., Richard, A. M., Laws, S. C., and Stoker, T. E. (2019). High-throughput screening and chemotype-enrichment analysis of ToxCast phase II chemicals evaluated for human sodium-iodide symporter (NIS) inhibition. *Environ. Int.* **126**, 377–386.

Westermark, K., and Westermark, B. (1982). Mitogenic effect of epidermal growth factor on sheep thyroid cells in culture. *Exp. Cell Res.* **138**, 47–55.

Yang, F., Ma, H., and Ding, X. Q. (2018). Thyroid hormone signaling in retinal development, survival, and disease. *Vitam. Horm.* **106**, 333–349.

Zimmermann-Belsing, T., Rasmussen, A. K., and Feldt-Rasmussen, U. (1998). Lack of thyroglobulin synthesis as an indicator of early random dedifferentiation of the Fischer rat thyroid cell line FRTL-5. *Scand. J. Clin. Lab. Invest.* **58**, 529–535.

Zoeller, R. T., and Crofton, K. M. (2000). Thyroid hormone action in fetal brain development and potential for disruption by environmental chemicals. *Neurotoxicology* **21**, 935–945.